Raman Spectroscopy for Monitoring of Microcystins in Water

Rebecca A. Halvorson

Thesis submitted to the faculty of the Virginia Polytechnic Institute and State University in partial fulfillment of the requirements for the degree of

Masters of Science Degree in Environmental Engineering

Peter J. Vikesland, Ph.D.
Amy J. Pruden, Ph.D
Andrea M. Dietrich, Ph.D.

December 6th, 2010
Blacksburg, VA

Keywords: Raman Spectroscopy, cyanotoxin, microcystin-LR, detection, DCDR, SERS, water

Raman Spectroscopy for Monitoring of Microcystins in Water

Rebecca A. Halvorson

ABSTRACT

Cyanobacterial blooms are of great concern to the drinking water treatment industry due to their capacity to produce microcystins and other cyanotoxins that are deadly to humans, livestock, pets, and aquatic life at low doses. Unfortunately, the strategies currently employed for cyanotoxin detection involve laborious analyses requiring significant expertise or bioassay kits that are subject to numerous false positives and negatives. These methods are incapable of providing rapid, inexpensive, and robust information to differentiate between the >80 cyanotoxin variants potentially present in an aqueous sample.

The use of Raman spectroscopy for identification and quantification of the ubiquitous cyanotoxin microcystin-LR (MC-LR) was examined. Raman spectra readily reflect minute changes in molecular structure, spectra can be collected through water or glass, portable Raman spectrometers are increasingly available, and through surface enhanced Raman spectroscopy (SERS) it is possible to achieve femto or picomolar detection limits for a variety of target species. Drop coating deposition Raman (DCDR) was successfully implemented for quantitation of 2-100 ng of MC-LR deposited in 2 μL of aqueous sample, even without the use of a specifically designed DCDR substrate or Raman signal enhancements. Reproducible MC-LR Raman spectra were observed for both fresh and aged DCDR samples, and the MC-LR Raman spectrum remained identifiable through a matrix of >80% DOM by mass. DCDR methods show tremendous potential for the rapid, simple, and economical detection of cyanotoxins in environmental matricies at environmentally relevant concentrations.

Table of Contents

Table of Figures

Table of Tables

Introduction

The compiled chapters describe research efforts directed towards the development of a method for identification and quantification of microcystins in water matricies. The first chapter describes the dangers of cyanotoxin presence in water supplies and the necessity for the development of novel monitoring technologies. Chapter two documents the author's research efforts to apply Raman methods for microcystin detection. Chapter three describes the potential utility of surface enhanced Raman spectroscopy (SERS) as a tool for environmental analyses. This chapter was published as a Feature article in *Environmental Science & Technology* on October 15th, 2010. The final chapter summarizes the engineering significance of the documented research efforts.

1

Cyanotoxins: The Looming Danger and the Necessity for Development of New Monitoring Technologies

The contamination of drinking water by cyanobacteria (blue-green algae) and their toxins is a significant health risk in both developed and developing regions of the world. Cyanobacterial blooms readily occur in freshwaters (e.g., reservoirs, lakes, rivers) used for drinking water supply when nutrient loads and temperatures are high and the water body is hydrologically stable (*1*), and they have even been identified in Blacksburg, VA (**Figure 1.1**). These blooms contain numerous cyanobacterial genera that can include *Microcystis, Anabaena, Anabaenopsis,* and *Nodularia,* among others (*2,3*). Although not all blooms are toxic, each of these genera has the potential to produce cyanotoxin byproducts that may elicit neurotoxic, hepatotoxic, cytotoxic, and gastrointestinal effects. The observation that cyanobacterial blooms can produce cyanotoxin byproducts that can exert a toxic effect at low doses has elicited great interest in protocols to quantify them both in raw and treated waters (*4*). Unfortunately, cyanotoxin monitoring programs are complicated by the existence of more than 90 cyanotoxin variants, many of which are structurally very similar (*5*). LC-MS-MS methods that can distinguish between these toxins are often too costly for routine monitoring by water utilities (*6*).

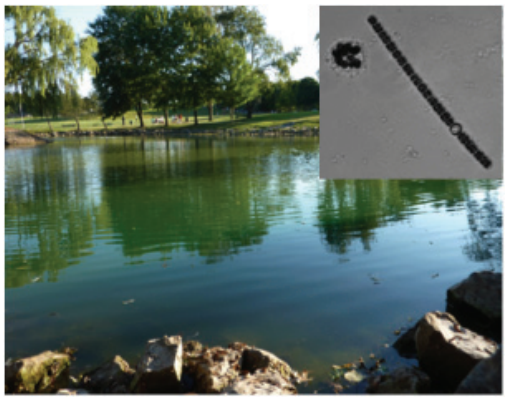

Figure 1.1. A cyanobacterial bloom on a Blacksburg, VA pond. The inset is an image of Anabaena (400×) as identified in the Vikesland lab.

Simpler bioassay kits that are available cannot distinguish between the variants and are subject to numerous false positive and negative results. Due to difficulties associated with existing cyanotoxin detection technologies, the widespread occurance of cyanotoxins, and the potent toxicity of the cyanotoxins, the EPA has included the microcystins, one of the most common cyanotoxin classes, on the 2009 drinking water contaminant candidate list 3 (CCL3; ref. *7*).

The cyclic heptapeptide microcystin (MC) toxins are one class of cyanotoxin that are of concern because they are common, inhibit protein phosphatase function thus causing liver failure, have tumor-promoting properties, and have been associated with primary liver cancer (Figure 1.2; refs. *8,9*). At present, over 80 microcystin variants have been identified (*5*) – these variants differ in terms of their peptide sequence, degree of methylation, and toxicity (*10*). Each microcystin has the general structure cyclo (D-Ala-L-X-D-MeAsp-L-Z-Adda-D-Glu-Mdha) where MeAsp is D-erythro-b-methylaspartic acid, Mdha is N-methyldehydroalanine, Adda is [(2S, 3S, 8S, 9S)-3-amino-9-methoxy-2,6,8-trimethyl-10-phenyldeca-(4E),(6E)-dienoic acid], and X and Z are variable amino acids. The hydrophobicity of the Adda group enables the microcystins to penetrate into hepatocytes, where they inhibit the activity of the serine-threonine protein phosphatases PP1 and PP2A (*11*).

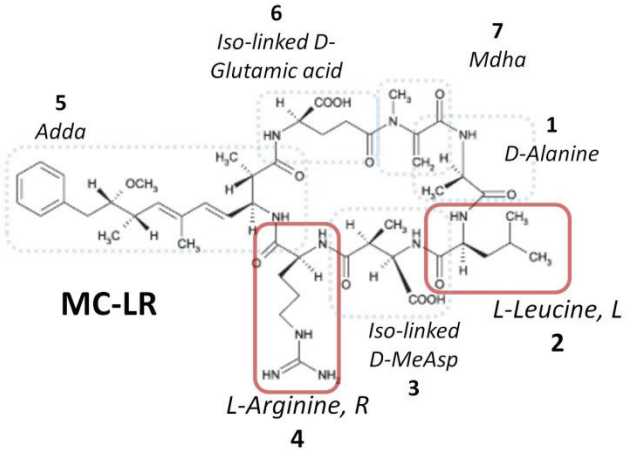

Microcystin	Amino acid 2	Amino acid 4
MC-LR	Leucine	Arginine
MC-RR	Arginine	Arginine
MC-LA	Leucine	Alanine
MC-LF	Leucine	Phenylalanine
MC-LY	Leucine	Tyrosine
MC-LW	Leucine	Tryptophan
MC-YR	Tyrosine	Arginine

Figure 1.2. Structures of microcystins**.**

Of the different microcystins, the most frequently detected (ranging from 23-94% of total MC content) and one of the most toxic is microcystin-LR (MC-LR, whose peptide chain contains leucine (L) and arginine (R) amino acids) (*3*). Other commonly observed congeners include microcystin-RR (MC-RR), microcystin-YR (MC-YR), and microcystin-LA (MC-LA; ref. *10*).

Unfortunately, conventional water treatment processes do not completely remove microcystins (*12-14*) and thus potential exposures via drinking water can result. A recent survey of U.S. lakes and water supply reservoirs indicated that 80% of the tested water bodies were positive for microcystin – clearly illustrating the ubiquity of cyanobacteria in the aquatic environment and the potential scope of the problem (*15*). In fact, it is estimated that the most likely routes by which one could be exposed to microcystins are via consumption of contaminated drinking water and exposure to contaminated recreational waters. Although the WHO suggested limit for MC-LR in drinking water is 1 nM (≈1 μg/L), dose-response experiments indicate that toxicity differs by variant with IC_{50} values of protein phosphatase inhibition for three tested microcystins and nodularin varying from 2.2-175 nM (*9*). Given the toxicity of the microcystins and their widespread presence, there is a dire need for water treatment utilities to possess an early warning system that provides either real-time or near-real-time warnings when microcystins are present in raw and treated waters.

Existing protocols for isolation and quantification of cyanotoxins

Typically, drinking water safety is maintained by analyzing source waters for either the presence of cyanobacteria or by measurement of the cyanotoxin concentration. Most current methods are expensive and time consuming or lack the sensitivity and repeatability to be applied

for large-scale drinking water monitoring. The following section discusses both the strengths and shortcomings of the current detection methods and demonstrates the dire need for improved method development.

Table 1.1. Existing detection methods for MC-LR. Method, method detection limit, and comments are included.

Method	MDL	Comments
Brine shrimp toxicity assay (*16*)	5-10 μg/kg	Measure of nonspecific toxicity, 24 hrs/sample (MDL= LD_{50})
TLC (thin-layer chromatography, ref. *17*)	1 μg/L	Requires 50 mL of sample, visual measure of microcystin presence
HPLC, UV-VIS detector (*3,18,19*)	1-10 ng*	Expensive standards, spectral overlap of different toxins
HPLC, PDA detector (*18*)	1-10 ng*	Spectral overlap of different toxins, $300 and 0.5-1 hr/sample**
LC-MS (*18*)	50 pg*	MS systems expensive, $400 and 0.5 hr/sample, fragment analyses
SPE and LC-MS/MS (*20,21*)	2.6 ng/L	for variant identification hindered by fragment overlap
MALDI-TOF-MS (*22*)	15 μg/L	Fast, matrix interference decreases sensitivity, expensive initial setup
SELDI-TOF-MS (*23*)	0.025 μg/L	Very sensitive, expensive initial setup, problematic analyte competition
ELISA (*24,25*)	0.2 μg/L	Kits available, $200/sample, antibody function can be difficult to predict
PPIA (*26,27*)	0.1 μg/L	Not sensitive for all microcystins, total toxicity, non-specific
MIPs (*28*)	0.2 μg/L	New technique with great potential for biosensors

*MDLs for HPLC correspond to mass registered by the instrument regardless of volume. Typical volumes are 10-25 μL. Extraction or concentration is necessary to increase sensitivity.
**All cost and time estimates provided by Lawton and Edwards, 2007 are listed as contract quotes. Analysis times exclude sample concentration and preparation (*18*)

Microcystins were historically monitored by whole organism (e.g., rodent, insect, crustacean) toxicity assays that are useful in terms of determining the overall toxicity of a water, but are time consuming and do not allow toxin identification (**Table 1.1**; refs. *29-31*). Given these limitations, most routine microcystin analyses are done using liquid chromatography with either UV-VIS diode-array or mass spectrometric (MS or MS/MS) detection (*3,32-37*). Microcystin quantification by UV-VIS entails comparison of retention times, UV-VIS spectra, and peak areas to commercially available standards. Unfortunately, most microcystins have identical UV-VIS profiles, so microcystin variants are usually expressed as equivalents of MC-LR. Quantitative analysis and unknown identification can be achieved with MS and MS/MS detection, however, the costs of these instruments preclude their widespread use (*4*).

The most promising methods for the rapid detection of microcystins rely upon molecular recognition events between microcystins and either antibodies or molecularly imprinted polymers (MIPs). The binding of a microcystin to one of these recognition agents can be monitored by various methods (e.g., electrochemistry or spectroscopy) and the resulting output can be correlated to the microcystin concentration (*11,38-40*). Although MIPs for microcystins have only recently been developed (*41,42*), the effectiveness of antibody based approaches is widely acknowledged. This utility is illustrated by the range of commercially available enzyme linked immunosorbent assays (ELISAs) currently on the market for microcystin analysis (e.g., SDI EnviroGard, EnviroLogix, Mistubishi ELISA). These ELISAs employ either monoclonal or polyclonal antibodies and exhibit varying affinities for different microcystin congeners (*43*). Unfortunately these assays are dependent upon the specificity of the antibody and as such are oftentimes subject to false positives.

The lack of sensitivity and specificity of the current microcystin detection methodologies are shortcomings that must be addressed to protect public health. **These observations suggest the dire need for a detection system for cyanotoxins that requires minimal operator training and that can provide rapid, accurate information about toxin concentrations.**

2

Drop Coating Deposition Raman (DCDR) for Microcystin-LR Identification and Quantitation in an Environmental Matrix

*Rebecca A. Halvorson and Peter J. Vikesland**

Department of Civil and Environmental Engineering and Institute of Critical Technology and Applied Science (ICTAS), Virginia Tech, 418 Durham Hall, Blacksburg, VA 24060-0246

ABSTRACT

A drop coating deposition Raman (DCDR) method was applied for analysis of 2-200 ng samples of microcystin-LR (MC-LR), a ubiquitous hepatotoxin secreted by cyanobacteria. Aqueous sample volumes of 0.5-20 μL generated sample deposits from which MC-LR Raman spectra could be obtained within seconds. Larger volume samples were not required to improve spectral resolution. Raman spectra of 2 μL "coffee-ring" deposits displayed distinct MC-LR Raman signals with high signal to noise in 1 s for a 200 ng (100 mg/L) sample and 300 s for a 2 ng (1 mg/L) sample. A linear correlation between Raman signal intensity and concentration was observed for 2-100 ng MC-LR samples analyzed over 50 s after normalization to fused silica glass background and a correction for laser power fluctuations. Reproducible DCDR MC-LR Raman spectra were collected from a fresh sample and a 6 mo old sample that had aged at room temperature in the dark. The presence of dissolved organic matter (DOM) does not preclude MC-LR identification in deposits of mixtures containing 3 μg DOM and 0.7 μg MC-LR. The DCDR

method for MC-LR identification can be applied following the routine filtration and SPE concentration steps commonly used prior to LC-MS-MS or ELISA detection of MC-LR. Raman based methods may facilitate faster sample throughput at a lower cost than traditional MC-LR detection methods.

INTRODUCTION

The contamination of drinking water by cyanobacteria (blue-green algae) and their neurotoxic, hepatotoxic, cytotoxic, and gastrointestinal toxins is a significant health risk in freshwaters (e.g., reservoirs, lakes, rivers) used for drinking water supply throughout the world (*1-4*). The World Health Organization has recommended an action level of 1 μg/L for microcystin-LR (MC-LR), one of the most commonly observed cyanotoxins. Unfortunately, MC-LR and the other cyanotoxins are not always completely removed by conventional drinking water treatment processes (*12-14*). Monitoring programs that have been implemented for cyanotoxin detection are hindered by the prevalence of more than 80 structurally similar forms of microcystin, the overlapping UV-Vis profiles of the microcystin variants, the common occurrence of false positives and negatives in immunoassays for microcystins, the lack of variant discrimination in enzyme inhibition assays, and the cost and expertise required to run LC-MS/MS instruments for large numbers of samples (*5,6*). There is a dire need for a detection method for microcystins that can provide rapid, reliable, cost effective, and accurate results. Such a method would allow monitoring programs to identify problematic water bodies before the public is exposed to the toxins.

Raman spectroscopy provides unique fingerprint spectra reflecting the molecular bond vibrations of polarizable molecules. Raman measurements can be made in aqueous matricies,

with portable spectrometers, through glass or plastic, and can be non-destructive under many circumstances (*44*). As a vibrational spectroscopic technique, Raman spectroscopy can identify subtle molecular differences such as chirality or local molecular environment, and can easily distinguish between the variant amino acids in different microcystins (i.e., leucine, arginine, alanine, phenylalanine, tryptophan; refs. *44-46*).

Historically Raman spectroscopy has not been applied for routine monitoring in the environmental field because of characteristically low intensity Raman signals and background fluorescence that can overshadow the analyte Raman signal. Recently, however, a drop coating deposition Raman (DCDR) method has facilitated successful analysis of human, bovine, and porcine insulin, lysozyme, glucose, glycans, taxanes, domoic acid, human tear fluid, and the synovial fluid of osteoarthritis patients, among other biomolecules at low concentrations, even in the presence of fluorescing matricies and mixtures (*47-52*). DCDR involves application of a few microliters of a sample solution to a substrate with a low solvent affinity and the absence of interfering Raman signals, absorbance, or adverse reflections. PTFE coated stainless steel, coated or uncoated glass, calcium fluoride slides, or gold foil have all been applied as DCDR substrates (*47,53,54*). As a drop of sample dries on a substrate, it leaves a "coffee-ring" of residue outlined by the pinned drop perimeter. This residue contains a majority of the sample conveniently concentrated at the drop edge (*47,55*). Raman analysis has shown that the DCDR sample drying process can segregate mixtures of analytes, fluorescing impurities, or buffer components from analytes such that the inner portion of the residue contains more soluble or less dense components such as sugars or buffer components, while the outer edge of the sample deposit is composed of denser proteins (*53,54,56*). Partial least squares (PLS) regressions and principal component analyses (PCA) can be used to distinguish DCDR spectra of human, bovine, and

porcine insulin as well as lysozyme, lactoferrin, and albumin proteins in human tear fluid (*48,53*). Concentrations of lysozyme, lactoferrin, and albumin in mixtures analyzed by DCDR were also predicted by PCA with root-mean-square errors of ~10% (*53*). The current study provides evidence that the drop coating deposition Raman method can be applied for rapid analysis and quantitation of samples containing MC-LR at quantities as low as 2 ng.

EXPERIMENTAL

MC-LR was purchased from Enzo Life Sciences (ALX-350-012) and used without further purification. Volumes of 0.5-20 μL containing 1-100 mg/L MC-LR were applied to fused silica glass substrates and allowed to air dry prior to analysis. Raman spectra of a dried 100 mg/L sample were collected on two instruments to optimize the instrument parameters for MC-LR Raman analysis: 1) A WiTec Alpha500R AFM Raman spectrometer with a UHTS300 spectrometer, DU 401 BR-DD CCD camera, 10× and 100× microscope objectives, 300 and 1200 gr/mm gratings, a TOPTICA XTRA diode 785 nm laser, and 633 nm He-Ne laser; and 2) A JY Horiba LabRAM HR 800 spectrometer with an Olympus BX-41 petrographic microscope, an Ancor electronically cooled CCD detector, 10× and 100× microscope objectives, 600 gr/mm grating, a 514 nm laser, and a 633 nm He-Ne laser. The UV-Vis spectrum of MC-LR was collected on a Varian Cary 5000 spectrophotometer between 200 and 900 nm. All subsequent Raman spectra were collected with the WiTec instrument, 785 nm laser, and 300 gr/mm grating (**Supporting Info, Figure 2.1** and **Supporting Info, Figure 2.2**).

Optical images and Raman spectra of sample deposits of interest were collected using 10× and 100× microscope objectives. Raman spectral maps 6 μm wide by 50-100 μm long were collected perpendicularly to the sample residue ridge with 1 s per spectrum, 2 spectra per μm

perpendicular to the drop edge, and 1 spectra per 2 μm parallel to the drop edge. The Raman laser probed approximately 0.5 μm laterally during each acquisition using the 785 nm laser and a microscope objective with a numerical aperture of 0.9. The shorter maps were collected for samples with narrower sample ridges formed by drop coating deposition.

Low concentration samples were also probed with 30 s and 300 s Raman spectral maps in the same region. The point of most intense Raman signal in each Raman spectral map was probed to obtain a single Raman spectrum based upon the average of 10 spectra collected over 5 s each. Additional Raman spectral maps of varying sizes were collected at points of interest. Samples were stored at room temperature in the dark after analysis and re-analyzed following storage to assess sample stability. Image J software was used to estimate drop sizes from optical images and sample ridge thicknesses from Raman spectral maps.

Dissolved organic matter was extracted from the Great Dismal Swamp in North Carolina by freeze drying swamp water that had eluted thru a cascade of filters down to a pore size of 0.45 μm. DOM was rehydrated and mixed thoroughly with MC-LR before application onto fused silica substrates.

RESULTS AND DISCUSSION

MC-LR drops of 0.5-20 μL at 100 mg/L concentrations dried in the characteristic "coffee-ring" shapes expected for the DCDR method (**Figure 2.1**; refs. *54,55*). The sample rings were systematically analyzed by collecting Raman spectral maps of the sample surface. The Raman spectrum of MC-LR alone was isolated by subtracting the fused silica glass Raman peaks from the spectrum of MC-LR (**Figure 2.1**).

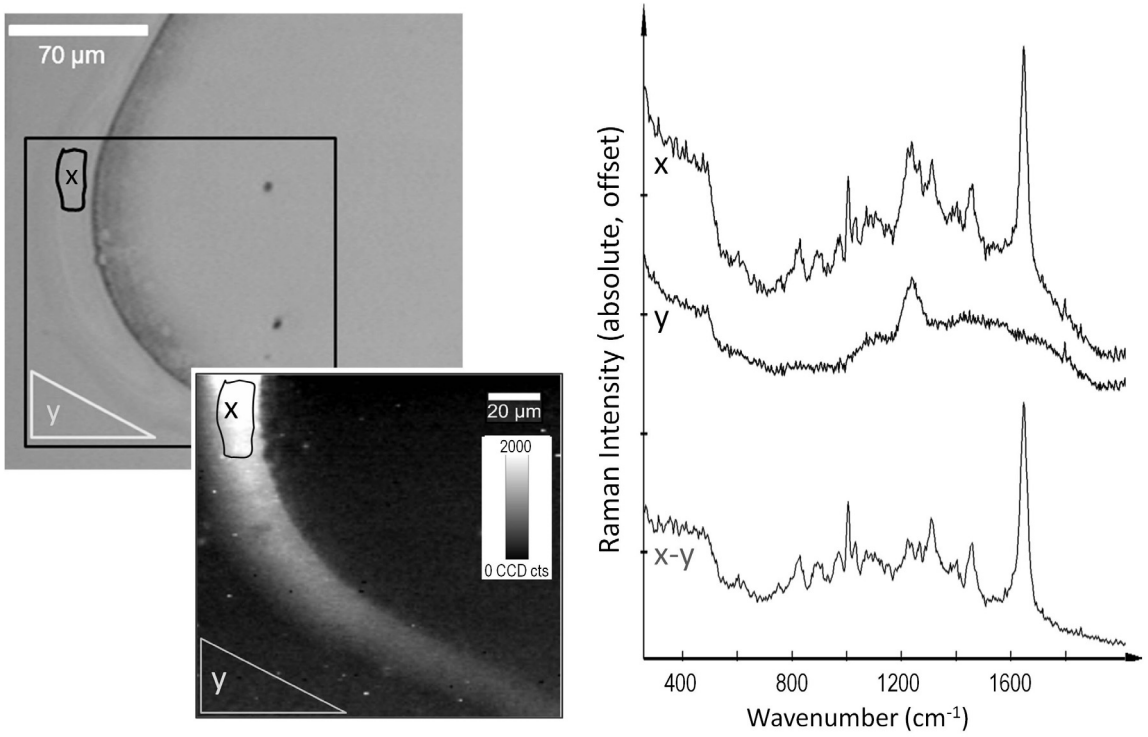

Figure 2.1. Optical images of DCDR samples display a "coffee-ring" residue deposit (left panel). MC-LR Raman signals are strong along the DCDR sample ridge (x). The region inside the ring and outside the ring exhibit fused silica glass Raman signals only (y) (center panel). The Raman spectral map of the region outlined in the optical image was created by tracking the intensity of the 1006 cm^{-1} Raman peak (produced by aromatic ring vibrations in the Adda portion of MC-LR; right panel). Thirty thousand spectra of 1 s acquisition/spectra were collected to create the spectral map.

Raman peaks were assigned to their corresponding molecular vibrational origins (**Table 2.1**). The most intense MC-LR Raman peaks include carboxylate vibrations observed at 1645 cm^{-1}, symmetric aromatic ring breathing modes at 1006 cm^{-1}, and CH_3/CH_2 modes at 1307 cm^{-1} (*57-59*). The fused silica substrate employed in these experiments was chosen because it exhibits minimal overlap with the MC-LR Raman spectrum, while simultaneously exhibiting Raman signals that could be used for signal normalization (**Table 2.2**). Experimental results suggest that the Raman intensities of fused silica peaks below 1140 cm^{-1} are largely dependent upon the instrument focal depth in relation to the sample (**Supporting Info, Figure 2.3**). Such changes

have also been observed for fused silica glass that was etched by laser irradiation; more intense signals were associated with the etched silica positions on the sample than the unmodified silica regions (*60*).

Table 2.1. MC-LR Raman peaks were assigned by comparison to literature spectra (*57-59*). Asterisks (*) indicate the most intense peaks.

Peak (cm^{-1})		**Molecular vibration**
751		CH_2 out of plane bending
828	*	C-H out of plane bending in benzoid ring
887	*	C-COOH stretch, methylene rocking
970	*	v(C-C) wagging, *p*(CH_3), δ(CCH)
1004	**	Phenylalanine C-C vibrations, symmetric ring breathing, methyl aspartic acid
1031	*	Phenylalanine C-H in plane bending, C-N stretching of proteins, C-C skeletal
1086	*	v(C-C) gauche
1204		Phenylalanine
1208-1214	*	Phenylalanine, aromatic ring vibrations
1200-300	*	Amide III
1259	*	Amide III
1307	**	CH_3/CH_2 modes (twist, wag, bend)
1384	*	CH vibrations
1453	*	C-H bending modes of proteins
1645	**	COO vibrations, water in L-lysine aqueous sample

Table 2.2. Fused silica Raman peaks were assigned by comparison to literature spectra (*60-63*).

Peak (cm^{-1})	**Molecular vibration**
400-500	Si-O-Si stretching and bending
~600	Three-membered ring structures of silica or –Si+ and –O-Si- defects
~800	Si-O-Si bending
1000-1140	Si-O stretching or stretching between disilicate and 3 bridging O atoms
970-1860	Silica, H_2O contained in the glass

The signal to noise ratio was consistently high and the peak positioning constant for ten Raman spectra collected in 5 s acquisitions and averaged for 0.5, 1, 2, 10, and 20 μL samples. This

finding is consistent with literature reports for DCDR of lysozyme and insulin (*47,54*). For MC-LR samples of 2 µL containing 2, 10, 20, 50, 100, and 200 ng of toxin, the Raman signal strength decreases as the analyte concentration decreases (**Figure 2.2**). Although the Raman signal of the glass becomes more intense than the MC-LR signal for the low concentration samples, spectral subtraction of the fused silica spectrum from the sample Raman spectrum produces clear MC-LR Raman spectra even for the 2 ng sample (**Supporting Info, Figure 2.4**).

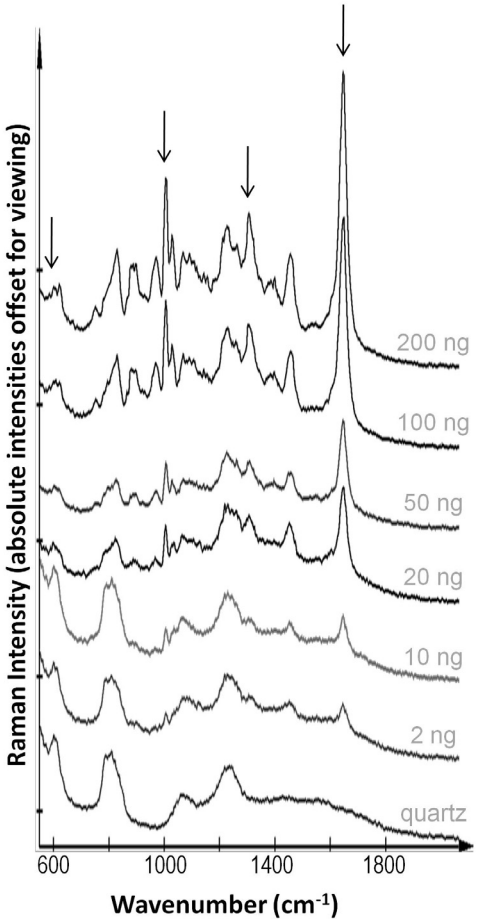

Figure 2.2. MC-LR DCDR spectra for 2 µL samples of 2-200 ng (1-100 mg/L concentrations). Highlighted peaks correspond to the 600 cm^{-1} glass peak, 1006 cm^{-1} aromatic MC-LR ring breathing, 1307 cm^{-1} CH_2 and CH_3 vibrations, and 1650 cm^{-1} COO^- vibrations. Each spectrum is the average of 10 acquisitions collected over 5 s each.

MC-LR Raman peak heights from nearby baseline minimums were monitored following signal normalization to create a calibration curve for 2-100 ng of MC-LR using Raman bands at 1006 cm^{-1}, 1307 cm^{-1}, 1457 cm^{-1}, and 1648 cm^{-1} (**Figure 2.3**). Confidence intervals suggest the trend line slopes are more accurate than the y-intercepts. A non-zero y-intercept is not surprising for any of the trend lines, especially for the 1648 cm^{-1} peak due to the contribution of fused silica substrate peaks to the MC-LR Raman spectra. The glass contributes less signal between 1006 cm^{-1} and 933 cm^{-1} than anywhere across the 970-1860 cm^{-1} silicate glass peak.

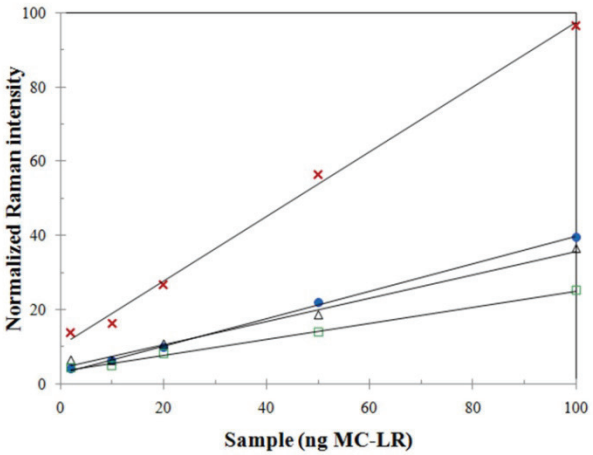

	Raman peak	Slope, 95% confidence	y-intercept, 95% confidence	R^2
●	1006 cm^{-1} – 933 cm^{-1}	0.40 ± 0.02	2.89 ± 1.13	0.999
Δ	1307 cm^{-1} -1515 cm^{-1}	0.32 ± 0.06	4.28 ± 2.95	0.990
X	1648 cm^{-1} -2000 cm^{-1}	0.87 ± 0.10	10.25 ± 5.01	0.996
□	1457 cm^{-1} - 1515 cm^{-1}	0.22 ± 0.02	3.49 ± 1.11	0.997

Figure 2.3. MC-LR calibration by DCDR method. Raman intensity was computed by subtracting the peak height from a nearby baseline minimum, normalizing the peak height to the fused silica background, and correcting the intensity for fluctuations in Raman laser power. Each point represents the average of 10 spectra of 5 s acquisitions collected from a 2 µL sample. Circles represent 1006 – 933 cm^{-1}, triangles signify 1307 – 1515 cm^{-1}, bars symbolize 1457 – 1515 cm^{-1}, and x corresponds to 1648 – 2000 cm^{-1}. In each case, the latter number indicates the nearby baseline minimum used to calculate the peak height.

Raman signal normalization was necessitated by variations in the focal plane of the Raman instrument during DCDR sample analysis. Raman spectra were collected after setting the focal plane to the depth that produced the most intense MC-LR Raman spectrum. This position was identified specifically for each sample by tweaking the focal plane of the Raman instrument and scanning across the sample rim in a direction perpendicular to the sample rim. Raman spectra

for 2-200 ng MC-LR were normalized to the fused silica glass background by dividing by a correction factor that fixed the height of the peak at 1515 cm^{-1} (corresponding to silica vibrations; ref. *63*) from the baseline at 2000 cm^{-1} to a constant value for all spectra. Fused silica glass signals below 1070 cm^{-1} varied with focal depth from the fused silica surface, and could not be used to normalize Raman spectra (**Supporting Info, Figure 2.3**). Behrens and co-workers also observed a dependence of Raman signal intensity on instrument focal depth for alkalialuminosilicate glass; T-O-T bending vibrations observed at 500 cm^{-1} were stable and could be used to normalize Raman spectra, while other silicate peaks varied with focal depth (*62*). The collected Raman spectra were also multiplied by a correction factor to normalize for day to day fluctuations in Raman laser power. The laser power correction factor was determined using 520 cm^{-1} and 942 cm^{-1} peak heights from the Raman spectrum of a silicon standard collected using maximum laser power for each analysis day. The peak height on analysis day one was divided by the peak height on analysis day two, and the ratios computed using the two different peaks were averaged to come up with a single correction factor describing the relative change in laser power.

A logical hypothesis for the strong correlation between MC-LR Raman signals and sample concentration is that the thickness of the deposited sample ring on the DCDR substrate correlates with sample concentration. AFM measurements of 3 µL DCDR samples of 14.3 to 1430 mg/L lysozyme suggest sample thickness decreases with a decrease in concentration, but a linear correlation was not observed when a PTFE coated stainless steel substrate was employed (*54*). The hydrophobicity of this substrate produces more condensed sample droplets than those deposited for the MC-LR experiments. A 0.77 µm thick sample ridge was observed for the 14.3 mg/L sample. Sample thickness of hyaluronic acid DCDR samples on Klarite SERS substrates from D3 Technologies Ltd. has also been estimated using thin film destructive interference

principles for 0.2 µL volume samples at 5, 1, and 0.25 g/L. Relative sample thickness was estimated to be ≈1.4 µm, ≈150 nm, and ≈150 nm respectively (*64*); however, the sample volume was much lower than those used in the MC-LR studies. Zhang et al. estimated insulin DCDR samples from 10 µL of 100 µM insulin (~57 mg/L) to be on the order of 10 µm thick on gold foil substrates.

The toxicity of MC-LR makes AFM measurements of MC-LR DCDR sample deposit thickness hazardous, so instead the approximate sample thickness was calculated using estimates of drop perimeters from optical images of the DCDR sample drops, sample ridge widths estimated from Raman spectral maps, and assumptions of MC-LR size and volume estimated from molecular models of MC-LR (downloaded from the Protein Data Bank, PDB file lfjm.pdb). MC-LR DCDR sample ridge thicknesses was computed to be between 2.4 and 0.2 µm (**Table 2.3**). However, drops were not of uniform shape, so these estimates contain a significant margin of error. Nonetheless the drop area did not correlate with concentration. Raman spectral maps suggest the width of the sample ridge decreased with decreasing concentration (though the sample ridge width was also not uniform), and this trend was reflected in the ridge thickness calculations.

Table 2.3. Computed sample ridge thickness for optimal Raman signal.

Mass (ng)	Edge width at Raman map (µm)	Image J measured drop area (µm^2)	Image J measured drop perimeter (µm)	Calculated thickness at ridge (µm)
200	16	3.0E+06	6300	2.4
100	12	5.1E+06	8100	1.3
50	10	2.8E+06	6000	1.0
20	5	2.7E+06	6000	0.8
10	7	4.9E+06	8200	0.2
2	2	3.0E+06	6500	0.2

* Assumes MC-LR volume of 2 nm^3 and a uniform drop edge.

The strength of the correlation between concentration and Raman intensities, the previous success of DCDR for the predictions of sample concentration, and the concentration levels that DCDR can observe suggest the DCDR method could be used for quantitation of MC-LR in pure samples (*53,65*). Solid phase extraction (SPE) using octadecyl silanised (C18) cartridges is routinely employed as a pre-concentration or sample purification step for analysis of plant, animal, or complex water samples containing MC-LR (*16*); in fact, an ISO standard (ISO 20179:2005) exists for reverse-phase SPE and HPLC of microcystins-LR, -RR, and –YR (*66*). Although Raman spectrometry is not often thought of for analysis of trace contaminants in water samples, SPE pre-concentration would allow DCDR to be employed for microcystins in environmental samples. If one were to analyze a sample containing 1 μg/L of MC-LR (the suggested WHO limit for drinking water), 500 mL of a sample could be extracted by filtration and SPE. Assuming high SPE recoveries which are not uncommon (*67*), approximately 0.5 μg of toxin would be eluted and rehydrated in a small volume of water, leaving concentrations well above 1 mg/L for DCDR analysis.

MC-LR DCDR sample aging. Sample stability was examined by collecting Raman spectra of DCDR samples that had been stored at room temperature in the dark after drop coating deposition on fused silica glass (**Figure 2.4**). Spectra are largely similar; however, an increase in the wavenumber of the 1006 cm^{-1} symmetric ring breathing peak and a decrease in the intensity of the 1648 cm^{-1} peak occur as samples age. These peaks correspond to symmetric aromatic ring breathing in the Adda group and C=O vibrations in MC-LR, although water O-H bending modes are also observed around 1650 cm^{-1} (*68*). Considering the stability and persistence of MC-LR in aquatic environments (*69,70*), significant degradation at room temperature is not expected. Instead, desiccation of the sample is a likely cause of the changes observed in the Raman

spectrum with aging. Most protein DCDR spectra resemble solution phase spectra (*47,54*), potentially due to the formation of a "glassy skin" at the surface of the deposited DCDR sample ring that keeps the sample under the surface well hydrated over short timescales (*71*). Zhang et al. also observed stable Raman spectra of lysozyme DCDR samples stored at 0° C for three weeks, and the lysozyme spectrum continued to resemble the aqueous phase spectrum following the storage period (*47*). Sample drying could cause a decrease in H_2O vibrations as observed at 1650 cm^{-1} as well as a shift in the position of the 1006 cm^{-1} peak (*59,72*). The Adda side chain of MC-LR resembles phenylalanine, for which symmetric ring breathing vibrations are observed in the region of 1000-1008 cm^{-1}, with the peak position shifting for different proteins; it is not unreasonable to assume the position of this peak is affected by the hydration state of the molecule.

Effects of DOM on MC-LR DCDR. An experiment was conducted to determine if the presence of DOM overshadows the MC-LR Raman signal during DCDR analysis. Mixtures of 1:1 and 1:5 MC-LR and DOM by mass were prepared and DCDR spectra collected. MC-LR was clearly identified in the deposited sample residue in every case (**Figure 2.5**), although regions of fluorescence were more common in the sample with the greatest amount of DOM. DCDR has been well established as a more effective method of fluorescence reduction than photobleaching

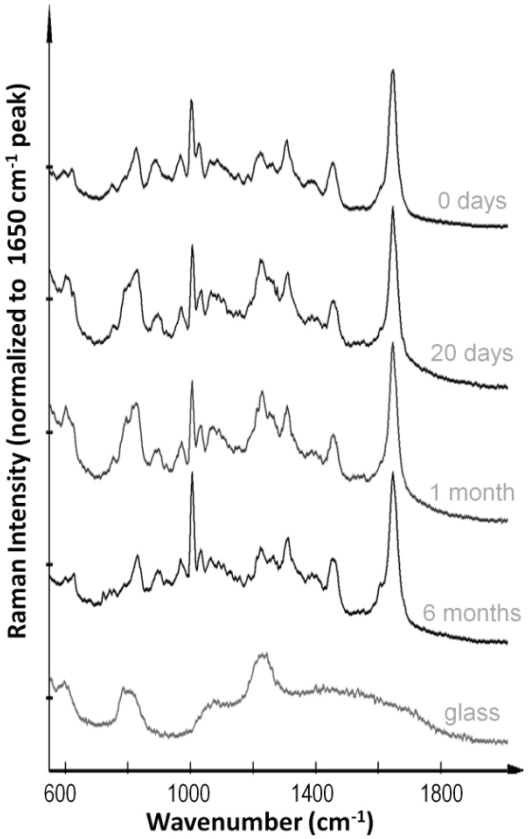

Figure 2.4. MC-LR DCDR sample aging. Raman spectra collected on fresh samples are compared with samples collected after an aging period of 20 days, 1 mo, and 6 mo. Spectral subtractions suggest small amounts of variation occur in the 1006 and 1648 cm^{-1} peaks.

for extended amounts of time (*56*). The drying process also can facilitate segregation of impurities or mixture components (*54,56*). Separation of mixture components during DCDR sample drying occurs due to differences in mass or the size of the solution components, solubilities, crystallization kinetics, or free energies of pure solids in comparison to solid solutions (*56*).

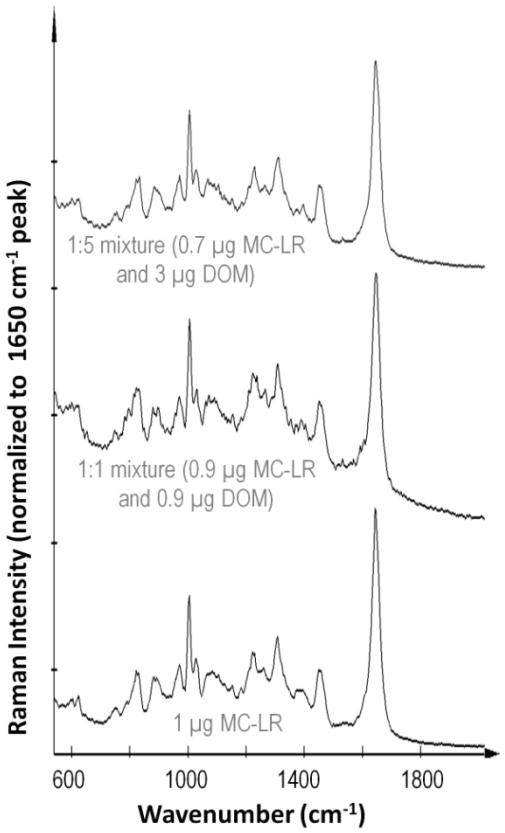

Figure 2.5. Raman spectra of MC-LR mixed with DOM at ratios of 1:5, 1:1, and 1:0 MC-LR: DOM by mass. Samples contain 0.7 µg MC-LR and 3 µg DOM, 0.9 µg MC-LR and 0.9 µg DOM, and 1 µg MC-LR with no DOM. Regions with intense MC-LR Raman signal were located by conducting Raman scans across the surface of the largely fluorescing samples.

FUTURE OUTLOOK

DCDR identification of MC-LR is successful in sample volumes of 0.5 µL and greater; larger volumes do not produce better Raman spectra. Linear correlations between Raman signal intensity and sample concentration were observed for 2 µL samples containing 2-100 ng of MC-LR after signal normalization to substrate background spectra and laser power. DCDR sample prep is conducive to the analysis of impure samples; DOM presence within a sample does not hinder identification of MC-LR. SPE methods that are routinely employed before ELISA or LCMS detection of MC-LR may be beneficial for the analysis of especially complex MC-LR

samples by DCDR. However, further DCDR experiments should be conducted on microcystin mixtures and impure solutions to identify constituents that may hinder analysis. DCDR in conjunction with a SPE toxin concentration step will be capable of identifying MC-LR at concentrations below the WHO suggested limit for drinking water.

The success of DCDR in classifying similar types of insulin despite only one amino acid difference between the tested varieties suggests DCDR may be capable of identifying the composition of a mixture of microcystin variants (*48*). Furthermore, similar proteins observed in human tear fluid have not only been distinguished from one another, but concentrations were also successfully predicted (*53*). DCDR analysis of MC-LR could be applied following HPLC separation (*47*) or filtration and SPE for routine monitoring. Although Raman instruments may not yet be established in all environmental laboratories, their initial cost is more economical than LC-MS-MS systems, Raman methods require fewer laboratory consumables than ELISA and PPIA, and Raman methods can utilize portable field instrumentation. The potential utility of a Raman method for microcystin analyses may one day enable cyanotoxin monitoring at more frequent intervals, thus resulting in a more robust detection program that would allow utilities to quickly respond to elevated toxin levels and to adjust their treatment practices accordingly. DCDR should not be overlooked for its potential in cyanotoxin monitoring.

ACKNOWLEDGEMENTS

This work was supported by an EPA STAR graduate research fellowship to R.A.H. (F08B20329) and research grants from the Water Research Foundation (#4212) and the Virginia Tech Institute for Critical Technology and Applied Science (ICTAS).

SUPPORTING INFORMATION

Raman instrument parameters. Raman spectra of MC-LR obtained using 514, 633, and 785 nm laser excitation contained similar features with different resolutions, which can be explained by the detector sensitivity and instrument focal length (**Supporting Info, Figure 2.1**). The quantum efficiency of the CCD camera on the WiTec instrument reaches a maximum near 785 nm and is lower (< 85%) at 633 nm (*73*). Therefore, the instrument collects more intense signals with the 785 nm laser. The 514 nm spectrum displays clearer, sharper peaks because the JY Horiba instrument is a High Resolution Raman spectrometer; it has a focal length of 800 mm while most spectrometers have a focal length of 300 mm. The longer focal length increases the resolution by a factor of approximately three, allowing more accurate description of peak shapes and band position (*74*). The UV-Vis absorbance spectrum of MC-LR is free of any absorbance between 300 to 900 nm, suggesting that sample spectral resonance is minimal (**Supporting Info, Figure 2.2**). Such will be the case for most microcystins; most variants absorb only between 200 and 300 nm due to the Adda group that contains a conjugated diene that absorbs at 238 nm (*16*). Tryptophan containing microcystins also absorb at 222 nm, but this absorbance will not affect the Raman spectra collected with laser wavelengths 514, 633, or 785 nm. All subsequent spectra were collected on the WiTec system because of its ability to rapidly collect high quality spectral maps and the availability of the 785 nm laser. The 785 nm laser is less likely to burn samples than more powerful lower wavelength lasers, the CCD camera on the WiTec instrument is most sensitive to Raman signals in the vicinity of 785 nm, and the lowest acquisition times were required with the 785 nm laser.

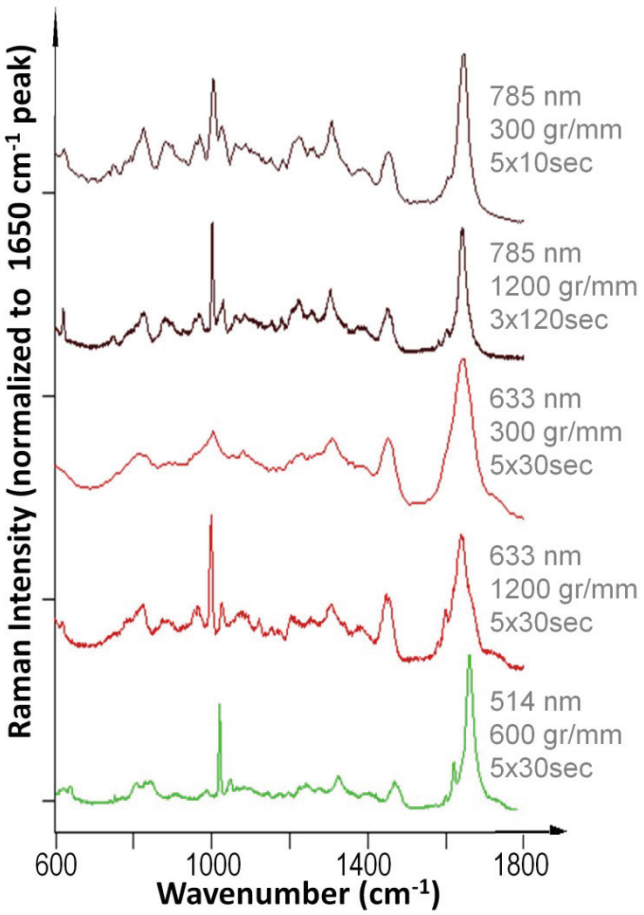

Supporting Info, Figure 2.1. MC-LR Raman spectra collected at a series of instrument parameters. WiTec Alpha 500 and JY Horiba LabRAM HR 800 spectrometers were used to collect spectra using a 100× microscope objective and the following parameters: A 785 nm laser and 300 gr/mm grating to collect the average of 5 acquisitions of 10 s each; 785 nm laser, 1200 gr/mm grating, and the average of 3 acquisitions of 120 s; 633 nm laser, 300 gr/mm grating, and the average of 5 acquisitions of 30 s; 633 nm laser, 1200 gr/mm grating, and the average of 5 acquisitions of 30 s; and 514 nm laser, 600 gr/mm grating, and the average of 5 acquisitions of 30 s. The Raman spectrum of MC-LR is affected by the Raman laser wavelength and grating choice; the 785 nm laser and 300 gr/mm grating produced the fastest spectra with sufficient resolution for peak identification.

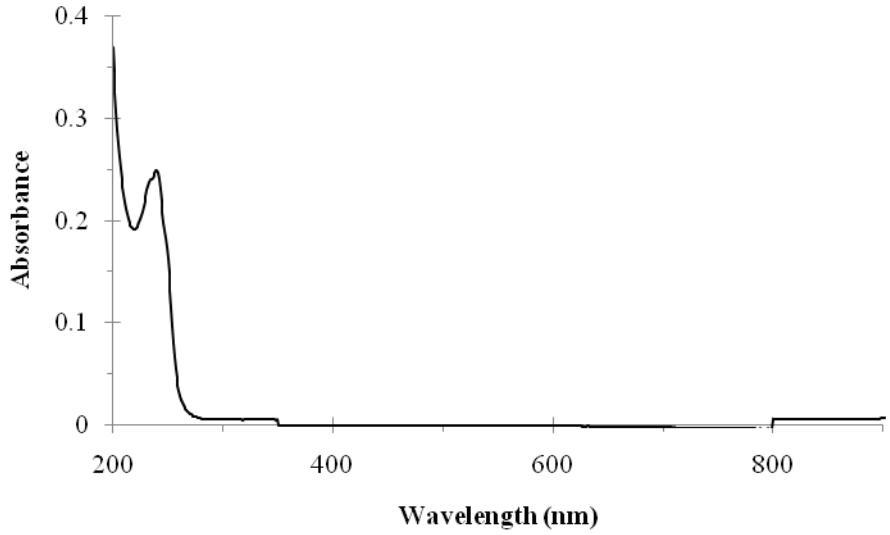

Supporting Info, Figure 2.2. UV-Vis of 4 mg/L MC-LR in a fused silica cuvette. The maximum absorbance occurs at 240 nm, and no absorbance is observed above 300 nm. Molecules that absorb the Raman laser wavelength will resonate upon laser contact and display more intense Raman signals than molecules that do not resonate; the lack of absorbance in the UV-Vis spectrum of MC-LR over 300 – 900 nm suggests resonance will not affect the Raman spectrum of MC-LR at any of the tested wavelengths.

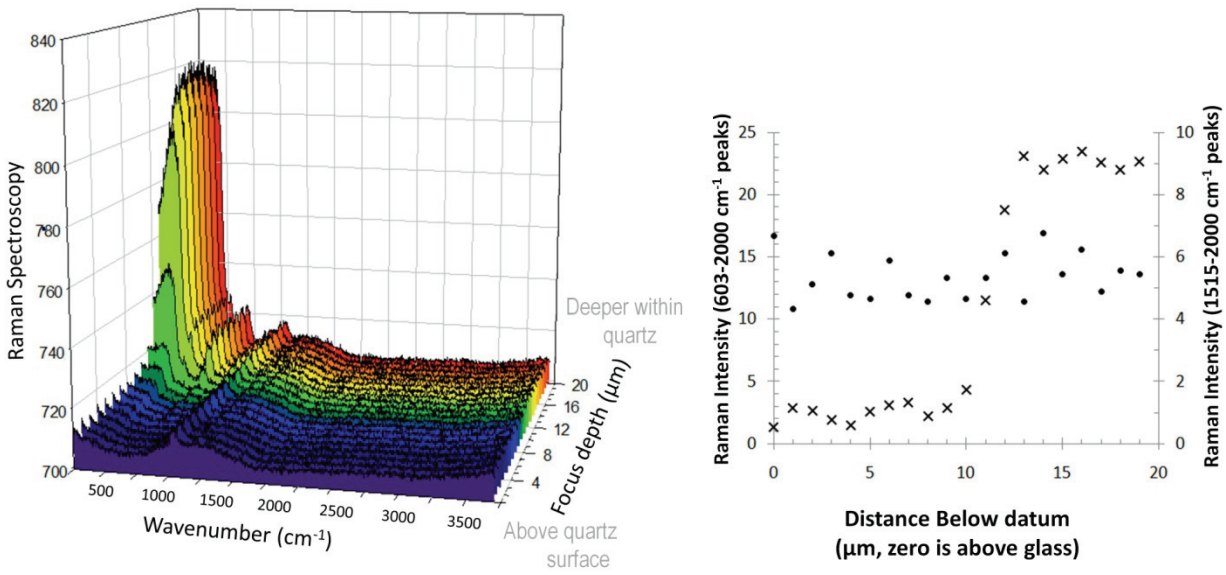

Supporting Info, Figure 2.3. Depth profile of fused silica glass Raman spectra. Spectra were collected at 1 μm intervals and plotted on a true y scale. Fused silica glass is an ideal substrate because it produces little Raman signal in the region of interest at its surface (600-1800 cm-1), but still provides some signal that can be used to normalize spectra. Normalization of MC-LR signals to glass background was achieved by fixing the peak height at 1515 cm^{-1} from the baseline at 2000 cm^{-1} to a constant value for all spectra. The peak at 603 cm^{-1} could not be used because it was affected by the focus depth in respect to the quartz, the peak at near 1200 cm^{-1} could not be used because it was overshadowed by MC-LR signals, but the 1515 cm^{-1} signal was stable across all quartz depths and it fell at a baseline in the MC-LR Raman spectrum.

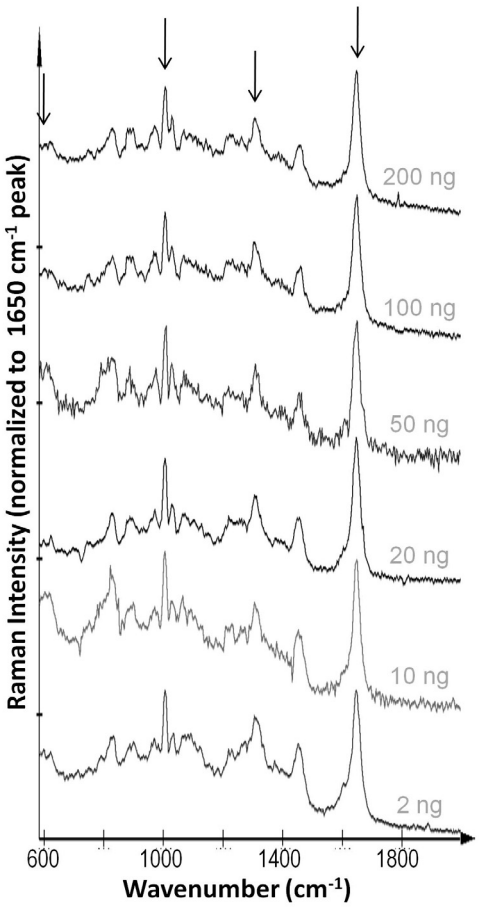

Supporting Info, Figure 2.4. DCDR spectra for 2 μL samples containing 200 – 2 ng of MC-LR. Highlighted peaks belong to 600 cm^{-1} glass peak, 1006 cm^{-1} aromatic MC-LR vibrations, 1307 cm^{-1} CH_2 and CH_3 vibrations, and 1650 cm^{-1} COO^- vibrations. Each spectra is the average of multiple acquisitions of 1 – 300 s each (200, 100, and 50 ng required 1 s acquisitions; the 20 and 10 ng samples required 30 s, and the 2 ng sample required 300 s acquisitions) from which the fused silica glass background signals have been subtracted. Spectra are normalized to the 1650 cm^{-1} peak.

3

Surface-Enhanced Raman Spectroscopy (SERS) for Environmental Analyses

*Rebecca A. Halvorson and Peter J. Vikesland**

Department of Civil and Environmental Engineering and Institute of Critical Technology and Applied Science (ICTAS), Virginia Tech, 418 Durham Hall, Blacksburg, VA 24060

Reproduced with permission from

Environmental Science & Technology **2010**, issue *44*, pp. 7749-7755.

Despite extensive efforts to protect public health, disease outbreaks still occur when toxic chemicals and microbial threats evade detection. Peanut butter and produce tainted with *Escherichia coli* 0157:H7, drinking water in Milwaukee, WI and Walkerton, ON (Canada) polluted by *Cryptosporidium*, surface waters contaminated by cyanotoxins, and mail laced with anthrax spores each represent an outbreak that may have been prevented with faster and more readily available pathogen or chemical detection methods. Although numerous techniques for contaminant detection in a variety of matrices exist, monitoring each analyte class generally requires specific instrumentation. Today, however, there is growing excitement about the potential use of surface-enhanced Raman spectroscopy (SERS) for simultaneous multiplex

detection of infectious and noninfectious contaminants in a range of environmental milieu. As currently envisioned, SERS is a platform for simple, fast, inexpensive, reliable, and robust methods to screen single or multiple contaminant classes simultaneously (*75-78*). Thousands of SERS publications document significant progress in achieving such a vision; however, as outlined herein several surmountable obstacles must be overcome to achieve these goals.

RAMAN SCATTERING AND SERS

As Raman and Krishnan first observed in 1928, natural molecular vibrations inelastically scatter light in a unique manner for every given molecular structure (*79*). This light is collected to create a Raman spectrum (**Figure 3.1a**). Raman measurements are simple to acquire, require little sample preparation, do not generally destroy samples or produce waste; spectra can be acquired through transparent glass, plastic, water, or solvent (*44*). However, due to the low strength of Raman signals, the technique has not gained significant traction as a tool for everyday environmental monitoring. The recent development of reproducible SERS substrates and methodologies has the potential to bring Raman based methods into more widespread use (*76*).

SERS, first observed in 1974, is an extension of normal Raman spectroscopy that relies on electronic and chemical interactions between the excitation laser, analyte of interest, and SERS substrate (*80*). Raman signal enhancements as high as 10^{14} can occur for resonant molecules found in "hot spots" on a SERS substrate due to combined electromagnetic (EM), charge transfer (CT), and resonance signal enhancement mechanisms (*81,82*). EM enhancement occurs when the incident laser excites surface plasmons (electrons at the metal surface that collectively oscillate upon excitation), thereby creating an electromagnetic field extending up to 20 nm from the metal and enhancing Raman signals of exposed molecules by an average of 10^4 (**Figure 3.1b**; ref. *83,84*). However, single molecule enhancements of 10^{11} can occur at nanoparticle junctions

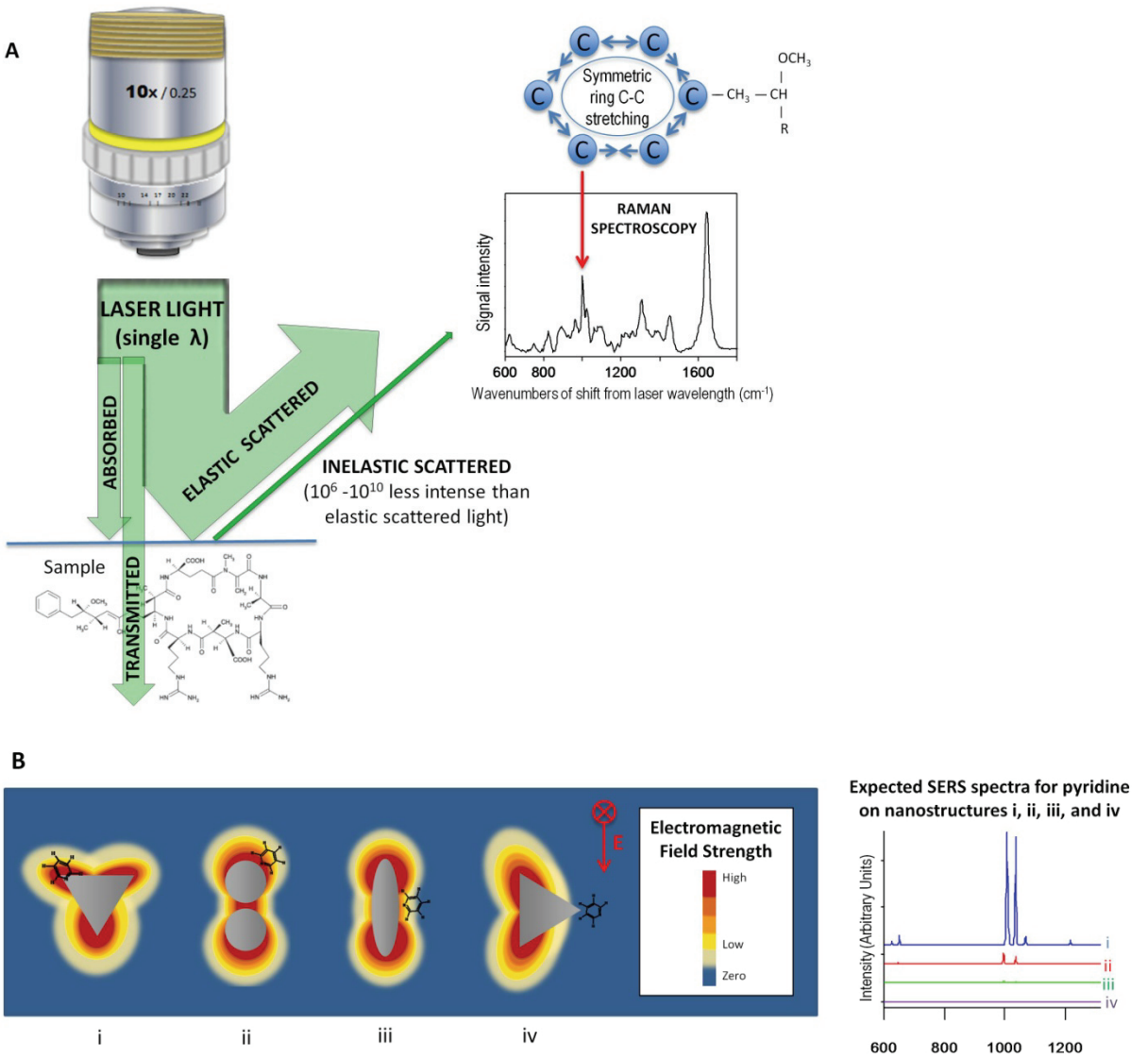

Figure 3.1. Raman Spectroscopy and SERS. **A)** Interaction between laser light and a molecule produces inelastic scattered light (light with a different wavelength than the incident light). Each molecular vibration uniquely shifts the wavelength of a portion of scattered light and is visible as a specific band in the Raman spectrum (*44*). **B)** Particle shape, size, and proximity to other particles affect the electromagnetic field (EM) that forms around a metal nanoparticle (adapted from ref. *85*). Expected SERS spectra for pyridine illustrate that signal enhancements are greatest for molecules subject to both EM and charge transfer (CT) (shape i), while no enhancement is expected if the analyte is positioned outside the EM field (adapted from ref. *86*).

where EM fields overlap (*81*). CT, the transfer of electrons between the analyte and metal surface, contributes an additional 10-100× enhancement when the analyte directly contacts the metal (*75,84,87*). Additional resonance enhancement is possible if the laser wavelength falls near an absorption wavelength of the sample (*84,87*). To achieve the lowest possible detection limits, all potential signal enhancements (EM, CT, and resonance) must be considered and maximized (**Figure 3.2** and **Table 3.1**).

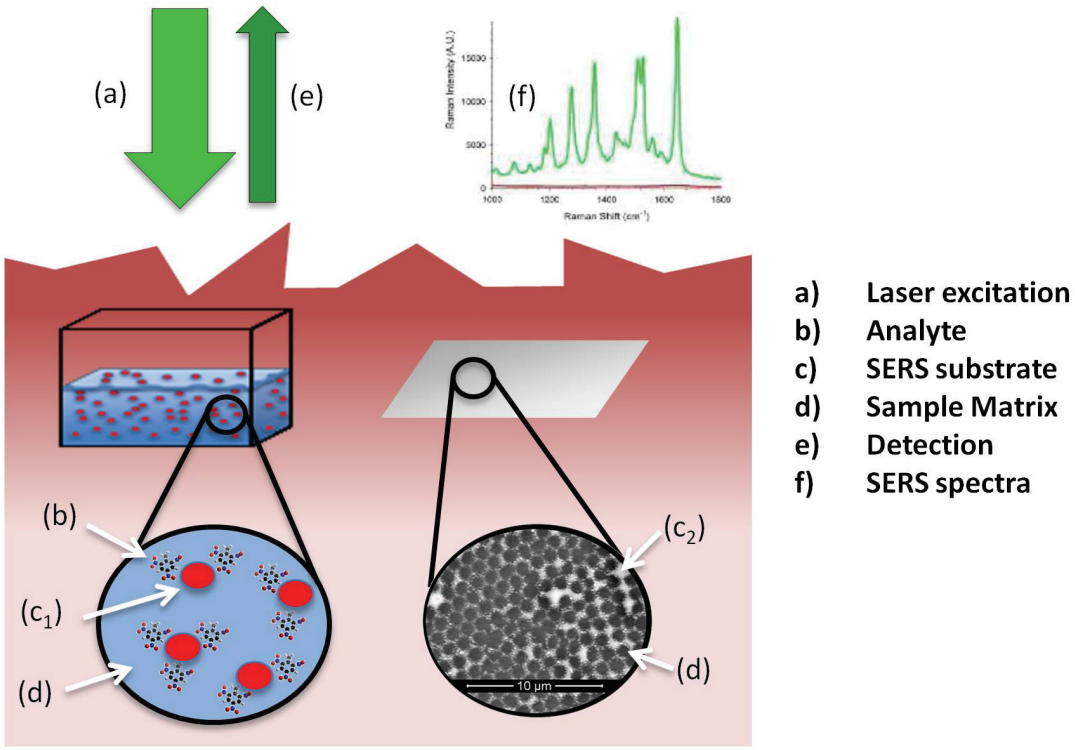

Figure 3.2. Components of a SERS measurement. Laser (**a**) illumination of an analyte (**b**) results in Raman signal emission and creates an EM field about the SERS substrate, commonly gold (Au) or silver (Ag) nanoparticles (**c_1**) or nanostructured surfaces (**c_2**; SEM courtesy of Weinan Leng, Virginia Tech) that are influenced by the sample matrix (**d**). The detector (**e**) collects inelastic scattered light from the sample. SERS occurs for RBITC using a 633 nm laser and 40 nm Au nanoparticles (**f**, green), but not 13 nm nanoparticles (**f**, red) because of the difference in the surface plasmon absorption band of the two particle sizes (*78*).

Table 3.1. Components of a SERS measurement.

	SERS step	Purpose	Design Considerations	Choices	Refs.
1)	Laser	Excites the analyte to produce Raman signals, generates EM field, enables resonance in the analyte.	Wavelength (consider plasmon absorption band of the SERS substrate, electronic transitions of analyte, and potential sample fluorescence) and power (maximize SERS signal while avoiding sample degradation).	Visible to IR lasers (488-1064 nm), 0-1000+ mW of power.	*44,87, 88*
2)	Analyte	Raman active analytes have polarizable bonds that vibrate and emit inelastic scattered light. SERS active molecules are polarizable upon interaction with a SERS substrate.	Polarizability in the presence of the SERS substrate, affinity for the SERS substrate, resonance at the laser wavelength, concentration, strength of polarizability with respect to background.	Endless possibilities. Any molecule that is polarizable upon interaction with a SERS substrate.	*44,75, 80,83*
3)	SERS Substrate	Provides EM field to enhance the Raman signal. Upon analyte contact, the substrate can also transfer charge to facilitate additional enhancement.	Size and sharpness of surface features, metal choice, surface functionalization, stability, synthesis complexity, reproducibility, biocompatibility, cost, wavelength of plasmon absorption band.	Gold, silver, copper, other metals; nanoparticles, ordered thin films, functionalized particles or surfaces.	*75,80, 83,89, 90*
4)	Sample Matrix and Analysis Condition	Can encourage or discourage interactions between analyte and SERS substrate, certain matrices quench SERS, solvent or fluorescent backgrounds can overshadow analyte spectra, experimental conditions may slightly shift peak locations and relative band heights.	Surface chemistry at SERS substrate, charge of analyte, influences of ions, peak locations of analyte in relation to solvent or background, laser wavelength corresponding to fluorescence, consistency between samples and experiments, homogeneity of samples.	Sample dissolved in water or organic solvent, dried sample, solid sample, ion addition, sample vessel material, sample flow through cell.	*44,81, 84,87, 91*
5)	Detection	Records Raman signals.	Wavelength range of detector, sensitivity, signal to noise ratio, response time, robustness, vulnerability to light.	CCD, multi-channeled photomultipliers, AlGaAs photocathodes, intensified CCDs, NIR detectors.	*44,88*
6)	Spectral Analyses	Peak area and band locations can be used for qualitative identification when compared to existing spectra. Peak areas and heights can be correlated to concentration for quantitative analyses.	Raman peak locations sensitive to bond's local environment, major peak shifts result from influence of SERS substrate on polarizability of analyte and formation of analyte-metal bonds, small position and intensity shifts occur when analyte favors a specific orientation to the metal surface, software packages available for analysis of large data sets, peak identification possible by comparing to existing spectra.	Peak identifications, principal component analysis, partial least squares (PLS), soft independent modeling of class analogies, and PLS–discriminant analysis are available when spatial and sample variability cause two spectra of the same sample to differ.	*44,83, 91-93*

Raman and SERS analytes. All polarizable molecules (molecules whose electron clouds are distorted by the electric field produced by a laser) generate Raman spectra. In general, non-polar groups and symmetric vibrations generate the strongest Raman bands, and isomerization or the proximity of electron withdrawing or donating groups shift the positions of Raman peaks - allowing similar analytes to be distinguished from one another. Concentration data is also embedded within relative peak heights or peak areas, although it is not always straightforward to extract (*44*). Importantly, the low polarizability index of water means that it produces negligible signal relative to more polarizable analytes dissolved or suspended within it, thus allowing aqueous contaminants to be observed by Raman spectroscopy (*84,94*). However, even species with weak Raman signals can be probed if the experiment is designed to accommodate lower intensity signals. For example, the extent of hydrogen bonding in water as determined by Raman spectroscopy can be used to infer temperature in a sample with an accuracy of ±0.1°C, but water also produces negligible background signal compared to 3 nM saxitoxin (*95,96*).

In theory any analyte can be detected by SERS if it is polarizable when it interacts with a SERS substrate. Even Raman-inactive molecules can become SERS-active if the EM field disrupts the normal symmetry of the analyte, the analyte is in resonance with the excitation laser, or CT occurs (*80*). SERS spectra are not always enhanced versions of Raman spectra; band positions migrate when metal-analyte bonds form, and relative band intensities shift when the analyte orients in a specific direction relative to the SERS substrate, thus allowing one portion of the molecule to be more highly affected by the EM field (*83,84,87*). Despite potential differences between Raman and SERS, the polarizable bonds within a molecule or complex are observed in both types of spectra, water exhibits a weak SERS signal, and although normal Raman can be hindered by background fluorescence signals 10^{14} times more intense than Raman signals

(produced when impurities or the sample itself absorb the laser line and re-emit it as the excited electrons return to the ground state), SERS substrates often provide nonradiative decay channels that quench fluorescence (*84*). These facts are critical for environmental applications of SERS as they allow acquisition of spectra of many classes of contaminants in aqueous matrices.

ENVIRONMENTAL APPLICATIONS

Although the complexity of SERS elicits some skepticism about the utility of the technique, its growing list of remarkable analytical achievements cannot be ignored (*76,78,82,91,92,97*). For example, in highly controlled environments, SERS can be used to detect contaminants at femtomolar concentrations over practical timescales (*82*). SERS is also capable of simultaneously detecting multiple contaminants of varying polarities and molecular weights, a feat that most existing detection strategies cannot achieve (*75,76,84*). Furthermore, SERS is exquisitely sensitive to subtle differences in material structure, allowing differentiation of similarly structured organic molecules and bacterial strains (*78,92,98*). Over the past 30 y, SERS has been used for quantitation and identification of organic and inorganic contaminants, pathogens, and nanomaterials in environmental samples (*75-77,93,97-99*). Detailed descriptions documenting the history of environmental applications of SERS, capabilities of SERS for single molecule detection, biowarfare agent detection, and medical applications are available elsewhere (*75,76,81,97*). Herein we focus on recent applications of SERS for qualitative identification and quantitative analysis of aqueous and airborne organic and inorganic contaminants and pathogens.

Aqueous and airborne organic and inorganic contaminants. SERS of aqueous species is relatively straightforward: the sample is dried onto a solid SERS substrate or dissolved in an aqueous phase containing nanoparticles. SERS of airborne samples requires an extra step to bring the analyte into contact with the SERS substrate. Airborne analytes may be deposited on

solid SERS substrates, pumped through impactors that direct samples into cuvettes containing aqueous nanoparticles, bubbled into nanoparticle solutions, or partitioned into water using free-surfaces on open fluidic devices (*100,101*).

Qualitative identification of TNT (2,4,6-trinitrotoluene), fullerenes, and numerous other compounds often rely on detection of a specific SERS spectrum to infer the presence of a contaminant (**Figure 3.3**a; refs. *82,98,102*). Impressively, the *in situ* identification of benzenethiol, 1-naphthylamine, and pyridine sorbed to humic acid was achieved simply by adding Au salt to humic acid. Humic acid acts as an oxidant and produces Au nanoparticles *in situ*. The background SERS spectrum for these nanoparticles provides an open spectral window through which SERS spectra of pollutants at 10^{-5} M concentrations are clearly visible (*98*).

Quantitative SERS is more challenging than qualitative, but can be achieved using internal standards that allow signal normalization or microfluidic cells that produce turbulent flow to mix samples and facilitate time-based signal averaging (**Figure 3.3b**). These methods reduce variability between measurements and create robust calibration curves. Such approaches have

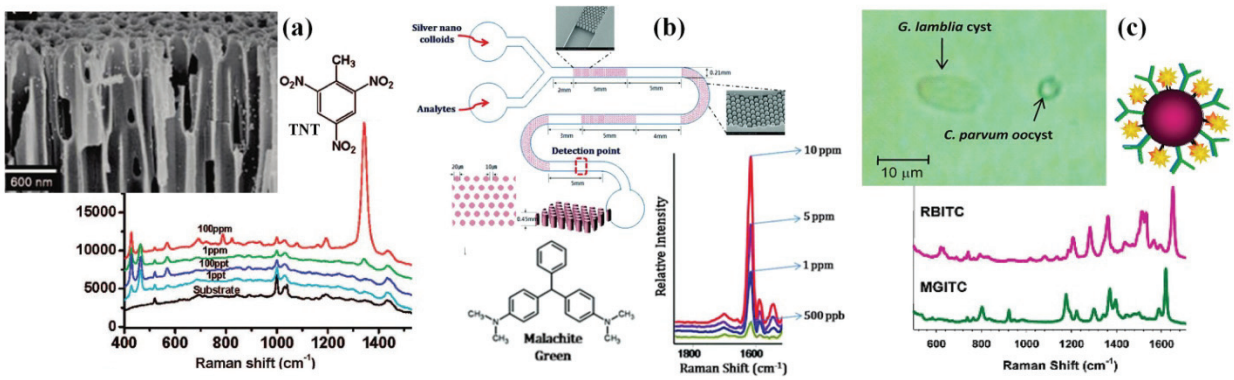

Figure 3.3. SERS Applications. A) Detection of TNT at zeptogram levels using alumina membrane pores coated with polyelectrolyte and Au nanoparticles, B) quantitation of malachite green fungicide solutions using a PDMS microfluidic channel and Ag nanoparticles, and C) identification of *Cryptosporidium* and *Giardia* using immunogold labels tagged with SERS-active dyes (*77,78,82*).

been used for quantitation of pesticides, nicotine, cyanide, methyl parathion, saxitoxin, dipicolinic acid (anthrax biomarker), and uranyl ions in aqueous samples (*91,96,99,103*).

Pathogen detection. SERS for pathogen detection is achieved by coating cells with a SERS-active material, reducing a noble metal at the cell wall to produce nanostructures, using a solid substrate, or marking pathogens with SERS-active immunotags; however, overcoming sample variablility can be challenging (*75,78*). The surface of a pathogen, which can vary in size from 10 nm for a small prion to many micrometers for protozoa, consists of a diverse array of biomolecules each with a characteristic Raman spectrum (*93,104*). SERS spectra reflect the region of the sample illuminated by the laser (the size of which is dependent upon the aperture of the microscope objective used to take the spectrum) and the surface features that associate with the SERS substrate. Variations in these parameters cause a pathogen to exhibit multiple SERS spectra. The effects of such variability can be minimized when SERS-active nanostructures associate with a specific biomolecule on the cell surface, microfluidic cells fully mix samples during spectral acquisition, or cells are deposited on solid substrates and SERS signals acquired over a large area are averaged (*104,105*). For example, SERS spectra for *E. coli* obtained using colloidal Ag exhibit band positions for flavin adenine dinucleotide (FAD) molecules because the nanosilver associates closely with flavins and thiol-containing flavoprotein pockets on the cell surface (**Figure 3.4**; refs. *75,100,104*).

Once sample variability is overcome, SERS can distinguish between viable and non-viable pathogens, Gram positive (*Listeria, Staphylococcus aureus, Bacillus subtilis, Bacillus amyloliquefaciens, Bacillus licheniformis*) and Gram negative (*Escherichia coli, Salmonella*) bacteria, and protozoa (*Cryptosporidium parvum*, *Giardia lamblia*) despite structural and biomolecular similarities (*76,92,93,104*). Spectral interpretation that allows species to be

distinguished from one another often involves principal component-discriminant function analysis or plots of ratios of SERS peak intensities (*92,93*). When surface features between pathogen species are not sufficiently unique to allow species determination, immuno-tags can be created that provide SERS substrates linked to both SERS-active molecules and antibodies for the targeted pathogen; such a scheme was recently implemented by our laboratory to tag *Cryptosporidium parvum* and *Giardia lamblia* (**Figure 3.3**c; ref. *78*).

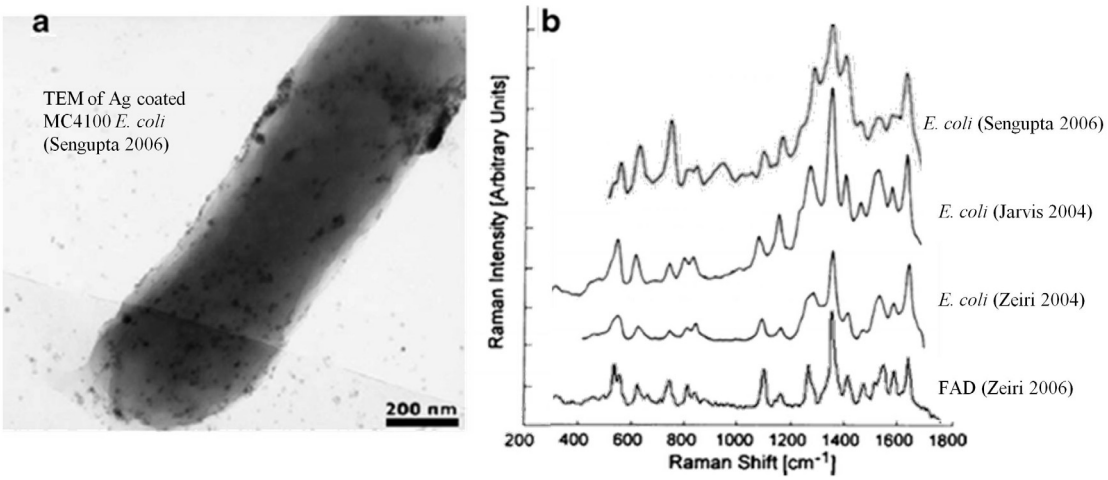

Figure 3.4. SERS spectra of *E. coli* from separate laboratories produced similar spectra with varied signal intensities (adapted from refs *75,104,105*). An external Ag coating on the cell membrane (*106*) and Ag nanoparticle coatings (*105,107*) facilitated the enhancements. FAD spectra compared to *E. coli* spectra demonstrate the preferential association of Ag nanostructures with FAD on the cell surface (*104*).

REMAINING CHALLENGES AND FUTURE OUTLOOK

Like any analytical technique, SERS has its own challenges, the greatest of which result from its strengths: SERS is not only sensitive to slight details of molecular structure, but also to local environment and molecular orientation at SERS substrates (*44,80*). Hence, it is not uncommon to acquire several completely distinct SERS spectra of a single sample within a fraction of a second, thus causing some SERS experiments to be considered highly variable. Slight changes in

SERS substrate features, extent of aggregation of nanosilver or nanogold, substrate surface chemistry, sample matrix chemistry, presence of impurities, analyte orientation, or analysis conditions can influence SERS spectra (*77,84,90*). Surface and sample matrix chemistry can be manipulated by adding ions to the sample, but ions can function as either SERS activators or quenchers, and their effects, which are difficult to predict, must be analyzed on a case by case basis (*81,99*). Unstable SERS spectra are also produced when signals from "SERS hotspots" dominate spectra or when laser exposure and thermal or photochemical mechanisms degrade analytes or SERS substrates over short timescales (*84,91*). Encouragingly, efforts to improve reproducibility have been successful. Precise quantitative SERS studies have been conducted using low laser power, internal standards that allow signal normalization throughout an experiment, microfluidic cells that create turbulent flow conditions to both mix the sample and allow an average over time to be measured, and reproducible SERS substrates that are currently being improved, tested, and commercialized (*75,90,91*).

SERS is also associated with its own specificity; although simultaneous detection of multiple contaminant classes is possible, it is not always straightforward to apply the SERS setup for one molecule to another with a similar structure, polarity, or molecular weight. Instead, the experimental parameters must often be carefully examined and modified for each SERS analyte. Analytes must be precisely matched to a compatible SERS substrate, excitation laser, and set of experimental parameters. Developing each specific SERS application requires trained laboratory personnel, research dollars, and patience in the laboratory, and only further study will allow SERS to achieve its full potential. Nevertheless, once developed, many SERS methods will tolerate simplification to allow practical application for routine monitoring.

Despite these stumbling blocks, SERS is rapidly evolving into a practical analytical tool that can be simultaneously applied to multiple analyte classes, and existing environmental applications are both plentiful and remarkable. Furthermore, SERS applications are not limited to the laboratory bench: microfluidic cell, lab-on-a-chip applications with portable Raman systems have facilitated quantitative field analyses for species such as dipicolinic acid and malachite green (a genotoxic antiseptic; ref. *77*). At the current rate of development of reproducible SERS substrates, microfluidic devices that reduce spectral variability, and practical applications for environmentally relevant analytical problems, SERS has great potential to become a rapid, reliable, and widespread technique. The future of SERS is bright indeed.

ACKNOWLEDGEMENTS

This work was supported by an EPA STAR graduate research fellowship to R.A.H. (F08B20329) and research grants from the National Science Foundation (BES-0606995) and ICTAS. The constructive comments of Dr. Weinan Leng are much appreciated.

4

Engineering Significance

Cyanotoxin poisonings occur worldwide, claiming the health and possibly the lives of cattle, dogs, wildlife, and humans. A few programs for routine cyanotoxin monitoring have been developed, but they are not as ubiquitous as the poisonings that occur (*6*). Monitoring programs must choose between lab kits such as ELISA that are readily available, but are only sensitive to select toxins, cannot distinguish between variant identities, and are linked to false positive and negative results, or LC-MS/MS methods that can distinguish between variants, but require expensive equipment and experienced lab technicians such that sample throughput is limited (*6,108*). Implementation of a Raman based approach for MC-LR detection and quantitation may allow rapid cyanotoxin variant identification at a lower cost than HPLC-MS/MS methods. Our DCDR experiments suggest the presence of DOM will not thwart Raman analysis, DCDR samples are stable even after aging, and only small volumes of sample are required for analysis. The detection limits of DCDR for MC-LR analyses have not yet been pushed to the limits, but DCDR can be easily implemented for samples containing 2 ng MC-LR in 2 μL. Filtration and SPE as conducted prior to implementation of existing ELISA or HPLC-MS/MS based detection methods for environmental samples could be applied to improve detection limits. If 1 L of water containing the WHO suggested limit of 1 μg/L MC-LR were extracted by SPE, 1 μg of toxin could be concentrated into 5 mL of methanol. This sample could then be dried and rehydrated in 100 μL of water, leaving a sample of 10 mg/L that could easily be examined by DCDR. Extraction processes implementing these volumes are not uncommon (*16,66,67,109*).

Raman signal enhancements induced by SERS have the potential to further improve the detection limits of Raman methods for MC-LR analyses. Quantitative SERS was applied for the cyanotoxin saxitoxin using silver nanoparticles with a limit of detection at 3 nM and limit of quantitation at 20 nM (*96*). Reproducible quantitative SERS methods can even be applied using portable Raman spectrometers (*77*).

Although Raman based detection is promising for identification of cyanotoxins, this work must be taken further to explore the detection limits of DCDR for MC-LR analyses, the ability of Raman spectroscopy to quantify and elucidate cyanotoxin identities in mixtures of toxin variants, and the success of analyzing samples containing additional impurities. However, it is the lack of Raman spectrometers in environmental laboratories that will be the largest barrier for application of Raman spectroscopy to routine monitoring. It may not be practical to purchase an instrument for which standard methods for environmental analyses do not yet exist, even if the Raman spectrometer is far from the most expensive instrument in the laboratory. Simpler field portable Raman spectrometers can be purchased with $12,000, but laboratory grade instrument costs start near $150,000. It will take time for the promising theories and successful experiments to ease the minds of those who may be able to implement these methods in the field but must first invest in an instrument. Nonetheless, Raman spectroscopy should not be overlooked for its utility in detecting and quantifying microcystins.

Literature Cited

1. Chorus, I., *Cyanotoxins: Occurrence, causes, consequences*. Springer-Verlag: Berlin, 2001; p 357.
2. Codd, G.A.; Morrison, L.F.; Metcalf, J.S., Cyanobacterial toxins: Risk management for health protection. *Toxicology and Applied Pharmacology* **2005,** *203*, 264-272.
3. Falconer, I.R., *Cyanobacterial toxins of drinking water supplies*. CRC Press: Boca Raton, Florida, 2005.
4. Sangolkar, L.N.; Maske, S.S.; Chakrabarti, T., Methods for determining microcystins (peptide hepatotoxins) and microcystin-producing cyanobacteria. *Water Research* **2006,** *40*, 3485-3496.
5. Van de Waal, D.B.; Verspagen, J.M.H.; Lurling, M.; Van Donk, E.; Visser, P.M.; Huisman, J., The ecological stoichiometry of toxins produced by harmful cyanobacteria: An experimental test of the carbon-nutrient balance hypothesis. *Ecol. Lett.* **2009,** *12*, 1326-1335.
6. Graham, J.L.; Loftin, K.A.; Kamman, N., Monitoring recreational freshwaters. *LakeLine* **2009,** *29*, 18-24.
7. EPA, Drinking water contaminant candidate list 3 (CCL3). *Fed. Regist.* **2009,** *74*, 51850-51862.
8. Carmichael, W.W., Cyanobacteria secondary metabolites-the cyanotoxins. *Journal of Applied Bacteriology* **1992,** *72*, 455-459.
9. Mountfort, D.O.; Holland, P.; Sprosen, J., Method for detecting classes of microcystins by combination of protein phosphatase inhibition assay and ELISA: Comparison with lc-ms. *Toxicon* **2005,** *45*, 199-206.
10. Perez, S.; Aga, D.S., Recent advances in the sample preparation, liquid chromatography tandem mass spectrometric analysis and environmental fate of microcystins in water. *Trac-Trends in Analytical Chemistry* **2005,** *24*, 658-670.
11. Campas, M.; Marty, J.L., Highly sensitive amperometric immunosensors for microcystin detection in algae. *Biosensors & Bioelectronics* **2007,** *22*, 1034-1040.
12. Blaha, L.; Marsalek, B., Dissolved microcystins in raw and treated drinking water in the czech republic. In *Cyanotoxins: Occurrence, causes, consequences*, Chorus, I., Ed. Springer-Verlag: Berlin, 2001; pp 212-216.
13. Gupta, S.; Giddings, M.; Sheffer, M., Cyanobacterial toxins in drinking water: A canadian perspective. In *Cyanotoxins: Occurrence, causes, consequences*, Chorus, I., Ed. Springer-Verlag: Berlin, 2001; pp 208-212.
14. Kruschwitz, C.; Chorus, I.; Heinzed, R.; Schlag, G.; Grobe, K., Elimination of microcystins in the rostock drinking water treatment plant. In *Cyanotoxins: Occurrence, causes, consequences*, Chorus, I., Ed. Springer-Verlag: Berlin, 2001; pp 217-225.
15. Carmichael, W.W., *Assessment of blue-green algal toxins in raw and finished drinking water*. AwwaRF and AWWA: Denver, CO, 2001; p 179.
16. McElhiney, J.; Lawton, L., Detection of the cyanobacterial hepatotoxins microcystins. *Toxicol. Appl. Pharmacol.* **2005,** *203*, 219-230.

17. Pelander, A.; Ojanpera, I.; Lahti, K.; Niinivaara, K.; Vuori, E., Visual detection of cyanobacterial hepatotoxins by thin-layer chromatography and application to water analysis. *Water Res.* **2000,** *34*, 2643-2652.
18. Lawton, L.A., C. Edwards, Proceedings of the interagency, international symposium on cyanobacterial harmful algal blooms. In *Adv. Exp. Med. Biol.*, Hudnell, H., Ed. 2007; pp 497-521.
19. Tillmanns, A.R.; Pick, F.R.; Aranda-Rodriguez, R., Sampling and analysis of microcystins: Implications for the development of standardized methods *Environ. Toxicol.* **2007,** *10*, 132-143.
20. Eaglesham, G.K.; Norris, R.L.; Shaw, G.R.; Smith, M.J.; Chiswell, R.K.; Davis, B.C.; Neville, G.R.; Seawright, A.A.; Moore, M.R., Use of hplc-ms/ms to monitor cylindrospermopsin, a blue-green algal toxin, for public health purposes *Environ. Toxicol.* **1999,** *14*, 151-154.
21. Zhang, L.; Xiaofei, P.; Yang, Z., Determination of microcystin-lr in surface water using high-performance liquid chromatography/tandem electrospray ionization mass detection. *Talanta* **2004,** *62*, 193-200.
22. Howard, K.L.; Boyer, G.L., Quantitative analysis of cyanobacterial toxins by matrix-assisted laser desorption ionization mass spectrometry *Anal. Chem.* **2007,** *79*, 5980-5986.
23. Gregson, B.P.; Millie, D.F.; Cao, C.; Fahnenstiel, G.L.; Pigg, R.J.; Fries, D.P., Simplified enrichment and identification of environmental peptide toxins using antibody-capture surfaces with subsequent mass spectrometry detection. *J. Chromatogr. A* **2006,** *1123*, 233-238.
24. Sheng, J.; He, M.; Shi, H., A highly specific immunoassay for microcystin-lr detection based on a monoclonal antibody. *Anal. Chim. Acta* **2007,** *603*, 111-118.
25. Rivasseau, C.; Racaud, P.; Deguin, A.; Hennion, M., Evaluation of an ELISA kit for the monitoring of microcystins (cyanobacterial toxins) in water and algae environmental samples. *Environ. Sci. Technol.* **1999,** *33*, 1520-1527.
26. Heresztyn, T.; Nicholson, B.C., Determination of cyanobacterial hepatotoxins directly in water using a protein phosphatase inhibition assay. *Water Res.* **2001,** *35*, 3049-3056.
27. Campas, M.; Marty, J.L., Highly sensitive amperometric immunosensors for microcystin detection in algae *Biosens. Bioelectron.* **2007,** *22*, 1034-1040.
28. Chianella, I.; Piletsky, S.; Tothill, I.; Chen, B.; Turner, A., Mip- based solid phase extraction cartridges combined with mip-based sensors for the detection of microcystin-lr. *Biosens. Bioelectron.* **2003,** *18*, 119-127.
29. Apeldoorn, M.E.v.; Egmond, H.P.v.; Speijers, G.J.A.; Bakker, G.J.I., Toxins of cyanobacteria. *Molecular Nutrition and Food Research* **2007,** *51*, 7-60.
30. Torokne, A.; Vasdinnyei, R.; Asztalos, B.M., A rapid microbiotest for the detection of cyanobacterial toxins. *Environmental Toxicology* **2007,** *22*, 64-68.
31. Marsalek, B.; Blaha, L., Comparison of 17 biotests for detection of cyanobacterial toxicity. *Environmental Toxicology* **2004,** *19*, 310-317.
32. Kankaanpaa, H.T.; Holliday, J.; Schroder, H.; Goddard, T.J.; Fister, R.v.; Carmichael, W.W., Cyanobacteria and prawn farming in northern new south wles, australia- a case study on cyanobacteria diversity and hepatotoxin bioaccumulation. *Toxicology and Applied Pharmacology* **2005,** *203*, 243-256.

33. Hoeger, S.J.; Shaw, G.; Hitzfeld, B.C.; Dietrich, D.R., Occurrence and elimination of cyanobacterial toxins in two australian drinking water treatment plants. *Toxicon* **2004,** *43*, 639-649.
34. Tillmanns, A.R.; Pick, F.R.; Aranda-Rodriguez, R., Sampling and analysis of microcystins: Implications for the development of standardized methods. *Environmental Toxicology* **2007,** *10*, 132-143.
35. Young, F.M.; Metcalf, J.S.; Meriluoto, J.A.O.; Spoof, L.; Morrison, L.F.; Codd, G.A., Production of antibodies against microcystin-rr for the assessment of purified microcystins and cyanobacterial environmental samples. *Toxicon* **2006,** *48*, 295-306.
36. Eaglesham, G.K.; Norris, R.L.; Shaw, G.R.; Smith, M.J.; Chiswell, R.K.; Davis, B.C.; Neville, G.R.; Seawright, A.A.; Moore, M.R., Use of hplc-ms/ms to monitor cylindrospermopsin, a blue-green algal toxin, for public health purposes. *Environmental Toxicology* **1999,** *14*, 151-154.
37. McElhiney, J.; Lawton, L.A., Detection of the cyanobacterial hepatotoxins microcystins. *Toxicology and Applied Pharmacology* **2005,** *203*, 219-230.
38. Zhang, F.H.; Yang, S.H.; Kang, T.Y.; Cha, G.S.; Nam, H.; Meyerhoff, M.E., A rapid competitive binding nonseparation electrochemical enzyme immunoassay (neeia) test strip for microcystin-lr (mclr) determination. *Biosensors & Bioelectronics* **2007,** *22*, 1419-1425.
39. Bouaicha, N.; Maatouk, I.; Vincent, G.; Levi, Y., A colorimetric and fluorometric microplate assay for the detection of microcystin-lr in drinking water without preconcentration. *Food and Chemical Toxicology* **2002,** *40*, 1677-1683.
40. Kim, Y.M.; Oh, S.W.; Jeong, S.Y.; Pyo, D.J.; Choi, E.Y., Development of an ultrarapid one-step fluorescence immunochromatographic assay system for the quantification of microcystins. *Environmental Science & Technology* **2003,** *37*, 1899-1904.
41. Chianella, I.; Piletsky, S.A.; Tothill, I.E.; Chen, B.; Turner, A.P.F., Mip-based solid phase extraction cartridges combined with mip-based sensors for the detection of microcystin-lr. *Biosensors & Bioelectronics* **2003,** *18*, 119-127.
42. Chianella, I.; Lotierzo, M.; Piletsky, S.A.; Tothill, I.E.; Chen, B.N.; Karim, K.; Turner, A.P.F., Rational design of a polymer specific for microcystin-lr using a computational approach. *Analytical Chemistry* **2002,** *74*, 1288-1293.
43. Metcalf, J.S.; Codd, G.A., Analysis of cyanobacterial toxins by immunological methods. *Chemical Research in Toxicology* **2003,** *16*, 103-112.
44. Pelletier, M.J., *Analytical applications of Raman spectroscopy*. Blackwell Science: Malden, MA, 1999.
45. Mukhejee, M.; Mukhopadhyay, A.; Charkraborty, T., Raman optical activity: A novel version of chiroptical spectroscopy. *Indian J. Phys.* **2008,** *82*, 987-1001.
46. Gelder, J.D.; Gussem, K.D.; Vandenabeele, P.; Moens, L., Reference database of Raman spectra of biological molecules. *JRSp* **2007,** *38*, 1133-1147.
47. Zhang, D.; Xie, Y.; Mrozek, M.F.; Ortiz, C.; Davisson, V.J.; Ben-Amotz, D., Raman detection of proteomic analytes. *Anal. Chem.* **2003,** *75*, 5703-5709.
48. Ortiz, C.; Zhang, D.; Xie, Y.; Davisson, V.J.; Ben-Amotz, D., Identification of insulin variants using Raman spectroscopy. *Anal. Biochem.* **2004,** *332*, 245-252.
49. Cipriani, P.; Ben-Amotz, D., Characterization of select members of the taxane family using Raman spectroscopy. *JRSp* **2005,** *36*, 1052-1058.

50. Djaoued, Y.; Balaji, S.; Priya, S., Non-resonance micro-Raman spectroscopic studies on crystalline domoic acid and its aqueous solutions. *Spectrochimica Acta Part A: Molecular and Biomolecular Spectroscopy* **2007,** *67*, 1362-1369.
51. Filik, J.; Stone, N., Analysis of human tear fluid by Raman spectroscopy. *Anal. Chim. Acta* **2008,** *616*, 177-184.
52. Esmonde-White, K.A.; Mandair, G.S.; Raaii, F.; Jacobson, J.A.; Miller, B.S.; Urquhart, A.G.; Roessler, B.J.; Morris, M.D., Raman spectroscopy of synovial fluid as a tool for diagnosing osteoarthritis. *JBO* **2009,** *14*.
53. Filik, J.; Stone, N., Drop coating deposition Raman spectroscopy of protein mixtures. *Analyst* **2007,** *132*, 544-550.
54. Ortiz, C.; Zhang, D.; Xie, Y.; Ribbe, A.E.; Ben-Amotz, D., Validation of the drop coating deposition Raman method for protein analysis. *Anal. Biochem.* **2006,** *353*, 157-166.
55. Deegan, R.D.; Bakajin, O.; Dupont, T.F.; Huber, G.; Nagel, S.R.; Witten, T.A., Capillary flow as the cause of ring stains from dried liquid drops. *Nature* **1997,** *389*, 827.
56. Zhang, D.; Mrozek, M.F.; Xie, Y.; Ben-Amotz, D., Chemical segregation and reduction of Raman background interference using drop coating deposition. *Appl. Spectrosc.* **2004,** *58*, 929-933.
57. Movasaghi, Z.; Rehman, S.; Rehman, I.U., Raman spectroscopy of biological tissues. *ApSRv* **2007,** *42*, 493 - 541.
58. Stewart, S.; Fredericks, P.M., Surface-enhanced Raman spectroscopy of amino acids adsorbed on an electrochemically prepared silver surface. *Spectrochim. Acta, Part A* **1999,** *55*, 1641-1660.
59. Chinsky, L.; Jolles, B.; Laigle, A.; Turpin, P.Y., Resonance Raman spectra of poly(l-lysine), aromatic amino acids, l-histidine and native and thermally unfolded ribonuclease a. *JRSp* **1985,** *16*, 235-241.
60. Reichman, W.; et al., Confocal fluorescence and Raman microscopy of femtosecond laser-modified fused silica. *J. Phys.: Condens. Matter* **2003,** *15*, S2447.
61. Mahapatra, M.K.; Lu, K., Effects of nickel on network structure and thermal properties of a new solid oxide cell seal glass. *J. Power Sources* **2008,** *185*, 993-1000.
62. Behrens, H.; Roux, J.; Neuville, D.R.; Siemann, M., Quantification of dissolved H_2O in silicate glasses using confocal microraman spectroscopy. *Chem. Geol.* **2006,** *229*, 96-112.
63. Walrafen, G.E.; Stone, J., Raman spectral characterization of pure and doped fused silica optical fibers. *Appl. Spectrosc.* **1975,** *29*, 337-344.
64. Esmonde-White, K.A.; Le Clair, S.V.; Roessler, B.J.; Morris, M.D., Effect of conformation and drop properties on surface-enhanced Raman spectroscopy of dried biopolymer drops. *Appl. Spectrosc.* **2008,** *62*, 503-511.
65. Xie, Y.; Zhang, D.; Ben-Amotz, D., Protein-ligand binding detected using ultrafiltration Raman difference spectroscopy. *Anal. Biochem.* **2008,** *373*, 154-160.
66. Meriluoto, J.A.; Spoof, L.E., Chapter 21: Cyanotoxins: Sampling, sample processing and toxin uptake. In *Cyanobacterial harmful algal blooms: State of the science and research needs*, Hudnell, K., Ed. Springer: New York, 2008; pp 483-499.
67. Feng, X.G.; Ding, Z.; Wei, T.; Yuan, C.W.; Fu, D.G., Identification and determination of microcystins in source water and waterbloom sample from meiliang bay, taihu lake, china. *Biomed. Environ. Sci.* **2006,** *19*, 225-231.

68. Ortiz, C.; Zhang, D.; Ribbe, A.E.; Xie, Y.; Ben-Amotz, D., Analysis of insulin amyloid fibrils by Raman spectroscopy. *Biophys. Chem.* **2007,** *128*, 150-155.
69. Shi, H.-X.; Qu, J.-H.; Wang, A.-M.; Ge, J.-T., Degradation of microcystins in aqueous solution with in situ electrogenerated active chlorine. *Chemosphere* **2005,** *60*, 326-333.
70. Jones, G.J.; Orr, P.T., Release and degradation of microcystin following algicide treatment of a microcystis aeruginosa bloom in a recreational lake, as determined by hplc and protein phosphatase inhibition assay. *Water Res.* **1994,** *28*, 871-876.
71. Kopecký Jr, V.; Baumruk, V., Structure of the ring in drop coating deposited proteins and its implication for Raman spectroscopy of biomolecules. *Vib. Spectrosc* **2006,** *42*, 184-187.
72. Ashton, L.; Dusting, J.; Imomoh, E.; Balabani, S.; Blanch, E.W., Shear-induced unfolding of lysozyme monitored in situ. *Biophys. J.* **2009,** *96*, 4231-4236.
73. WiTec, Witec alpha 500 user manual. 2008.
74. Lastek, Horiba Jobin-Yvon LabRAM hr high resolution Raman spectrometer; http://www.Lastek.Com.Au/content/view/233/748/. Accessed 7/29/2010.
75. Hering, K.; Cialla, D.; Ackermann, K.; Dorfer, T.; Moller, R.; Schneidewind, H.; Mattheis, R.; Fritzsche, W.; Rosch, P.; Popp, J., SERS: A versatile tool in chemical and biochemical diagnostics. *Anal. Bioanal. Chem.* **2008,** *390*, 113-124.
76. Golightly, R.S.; Doering, W.E.; Natan, M.J., Surface-enhanced Raman spectroscopy and homeland security: A perfect match? *ACS Nano* **2009,** *3*, 2859-2869.
77. Quang, L.X.; Lim, C.; Seong, G.H.; Choo, J.; Do, K.J.; Yoo, S.K., A portable surface-enhanced Raman scattering sensor integrated with a lab-on-a-chip for field analysis. *LChip* **2008,** *8*, 2214-2219.
78. Rule, K.; Vikesland, P., Surface-enhanced resonance Raman spectroscopy for the rapid detection of *Cryptosporidium parvum* and *Giardia lamblia*. *Environ. Sci. Technol.* **2009,** *43*, 1147-1152.
79. Raman, C.V.; Krishnan, K.S., A new type of secondary radiation. *Nature* **1928,** *121*, 501-502.
80. Moskovits, M., Surface-enhanced Raman spectroscopy: A brief perspective. In *Surface-enhanced Raman scattering*, Kneipp, K.; Moskovits, M.; Kneipp, H., Eds. Springer: Berlin, 2006; pp 1-17.
81. Qian, X.M.; Nie, S.M., Single-molecule and single-nanoparticle SERS: From fundamental mechanisms to biomedical applications. *Chem. Soc. Rev.* **2008,** *37*, 912-920.
82. Ko, H.; Chang, S.; Tsukruk, V.V., Porous substrates for label-free molecular level detection of nonresonant organic molecules. *ACS Nano* **2009,** *3*, 181-188.
83. Smith, W.E., Practical understanding and use of surface enhanced Raman scattering/surface enhanced resonance Raman scattering in chemical and biological analysis. *Chem. Soc. Rev.* **2008,** *37*, 955-964.
84. Haynes, C.L.; McFarland, A.D.; Van Duyne, R.P., Surface-enhanced Raman spectroscopy. *Anal. Chem.* **2005,** *77*, 338A-246A.
85. Hao, E.; Schatz, G.C., Electromagnetic fields around silver nanoparticles and dimers. *J. Chem. Phys.* **2004,** *120*, 357-366.
86. Muniz-Miranda, M.; Cardini, G.; Schettino, V., Surface-enhanced Raman spectra of pyridine and pyrazolide on silver colloids: Chemical and electromagnetic effects. *Theor. Chem. Acc.* **2004,** *111*, 264-269.
87. Aroca, R., *Surface-enhanced vibrational spectroscopy*. Wiley: Hoboken, NJ, 2006.

88. Asher, S.A.; Bormett, R., Raman instrumentation. In *Raman scattering in materials science*, Weber, W.H.; Merlin, R., Eds. Springer: Berlin, 2000; pp 35-54.
89. Banholzer, M.J.; Millstone, J.E.; Qin, L.; Mirkin, C.A., Rationally designed nanostructures for surface-enhanced Raman spectroscopy. *Chem. Soc. Rev.* **2008,** *37*, 885-897.
90. Lin, X.M.; Cui, Y.; Xu, Y.H.; Ren, B.; Tian, Z.Q., Surface-enhanced Raman spectroscopy: Substrate-related issues. *Anal. Bioanal. Chem.* **2009,** *394*, 1729-1745.
91. Bell, S.E.J.; Sirimuthu, N.M.S., Quantitative surface-enhanced Raman spectroscopy. *Chem. Soc. Rev.* **2008,** *37*, 1012-1024.
92. Liu, Y.; Chao, K.; Nou, X.; Chen, Y.-R., Feasibility of colloidal silver SERS for rapid bacterial screening. *Sens. Instrum. Food Qual. Saf.* **2009,** *3*, 100-107.
93. Jarvis, R.M.; Brooker, A.; Goodacre, R., Surface-enhanced Raman scattering for the rapid discrimination of bacteria. *Faraday Discuss.* **2006,** *132*, 281-292.
94. Orttung, W.H., Radius and polarizability of water from refractive index data *J. Phys. Chem.* **1963,** *67*, 503-504.
95. Davis, K.L.; Lee, K.; Liu, K.; Lanan, M.; Morris, M.D., Spatially resolved temperature measurements in electrophoresis capillaries by Raman thermometry. *Anal. Chem.* **1993,** *65*, 293-298.
96. Pearman, W.F.; Angel, S.M.; Ferry, J.L.; Hall, S., Characterization of the Ag mediated surface-enhanced Raman spectroscopy of saxitoxin. *Appl. Spectrosc.* **2008,** *62*, 727-732.
97. Baker, G.A.; Moore, D.S., Progress in plasmonic engineering of surface-enhanced Raman-scattering substrates toward ultra-trace analysis. *Anal. Bioanal. Chem.* **2005,** *382*, 1751-1770.
98. Álvarez-Puebla, R.A.; Dos Santos, D.S.; Aroca, R.F., SERS detection of environmental pollutants in humic acid-gold nanoparticle composite materials. *Analyst* **2007,** *132*, 1210-1214.
99. Bao, L.; Mahurin, S.M.; Haire, R.G.; Dai, S., Silver-doped sol-gel film as a surface-enhanced Raman scattering substrate for detection of uranyl and neptunyl ions. *Anal. Chem.* **2003,** *75*, 6614-6620.
100. Sengupta, A.; Brar, N.; Davis, E.J., Bioaerosol detection and characterization by surface-enhanced Raman spectroscopy. *J. Colloid Interface Sci.* **2007,** *309*, 36-43.
101. Piorek, B.D.; Lee, S.J.; Santiago, J.G.; Moskovits, M.; Banerjee, S.; Meinhart, C.D., Free-surface microfluidic control of surface-enhanced Raman spectroscopy for the optimized detection of airborne molecules. *Proc. Natl. Acad. Sci. U. S. A.* **2007,** *104*, 18898-18901.
102. Luo, Z.; Fang, Y., Investigation of the mechanism of influence of colloidal gold/silver substrates in nonaqueous liquids on the surface enhanced Raman spectroscopy (SERS) of fullerenes c60 (c70). *J. Colloid Interface Sci.* **2006,** *301*, 184-192.
103. Lee, S.; Choi, J.; Chen, L.; Park, B.; Kyong, J.B.; Seong, G.H.; Choo, J.; Lee, Y.; Shin, K.-H.; Lee, E.K.; Joo, S.-W.; Lee, K.-H., Fast and sensitive trace analysis of malachite green using a surface-enhanced Raman microfluidic sensor. *Anal. Chim. Acta* **2007,** *590*, 139-144.
104. Zeiri, L.; Efrima, S., Surface-enhanced Raman scattering (SERS) of microorganisms. *Isr. J. Chem.* **2006,** *46*, 337-346.
105. Sengupta, A.; Mujacic, M.; Davis, E., Detection of bacteria by surface-enhanced Raman spectroscopy. *Anal. Bioanal. Chem.* **2006,** *386*, 1379-1386.

106. Zeiri, L.; Bronk, B.V.; Shabtai, Y.; Eichler, J.; Efrima, S., Surface-enhanced Raman spectroscopy as a tool for probing specific biochemical components in bacteria. *Appl. Spectrosc.* **2004,** *58*, 33-40.
107. Jarvis, R.M.; Brooker, A.; Goodacre, R., Surface-enhanced Raman spectroscopy for bacterial discrimination utilizing a scanning electron microscope with a Raman spectroscopy interface. *Anal. Chem.* **2004,** *76*, 5198-5202.
108. Carmichael, W.W., Assessment of blue-green algal toxins in raw and finished drinking water. *American Water Works Association Research Foundation* **2001**.
109. Ming Dai; Ping Xie; Gaodao Liang; Jun Chen; Donghu, H.L., Simultaneous determination of microcystin-lr and its glutathione conjugate in fish tissues by liquid chromatography–tandem mass spectrometry *J. Chromatogr. B* **2008,** *862*, 43-50.